ANÁLISIS DE CONECTIVIDAD FUNCIONAL DE LA DINÁMICA NEUROENERGÉTICA DEL TDAH.

(Functional Connectivity Analysis of Neuroenergetic Dynamics for ADHD)

Daniela Ospina Toro
Cod: 1088274042

Directores

PhD. Óscar A. Henao Gallo

PhD. Antonio Escobar Zuluaga

Programa De Maestría En Ingeniería Eléctrica
Facultad De Ingeniería Eléctrica, Electrónica, Física Y Ciencias De La Computación
Universidad Tecnológica De Pereira
Pereira
2016

Dedication:

I dedicate my research to my mother and my grandparents for being always supportive.

Acknowledgements:

To Professor Oscar Henao for his help with the mathematical and statistical fundaments. To Professor José Fernando López for help us to contact the school where the procedure was performed and for believe in this project. To Ms. Gloria for being supportive and help us approaching to the children. To Professor Felipe Parrado for helping me in the construction of the hypothesis and the psychological fundaments. To Professor Antonio Escobar for supporting us during the whole process. To Colciencias for founding the first stage of this research. To the Master in Electrical Engineering for providing an space for developing this research. To the reviewers for taking their time for reading this document, specially to Professor Stephen Coombes.

Table of Contents

1 Abstract

A fast and economic pilot study for measuring the neuroenergetic dynamics in an ADHD-diagnosed sample is performed. Based in a simplified connectome version, a graph theory application for neural connectivity, the performance and subjective states are linked through brain activity analysis during a behavioral attention test.

ADHD is a neurobehavioral disorder related to a deficient filtering of stimuli, inefficacy performing in sustained activities and difficulties responding to unpredictable situations. There are two main strategies to evaluate this disorder: (1) behavioral tests and (2) neural biomarkers.

Behavioral tests provide a criterion for classifying responses in a collection of tasks, looking for unstructured and inconsistent responses to given instructions or rules. Hyperactivity, inattention and impulsivity are some criteria analyzed.

By the other hand, neural biomarkers are measurable indicators for particular states or diseases set up from EEG data. Since 2013, the theta/beta ratio was accepted as the ADHD biomarker, suggesting a misbalance of electrical brain activity. In this study, brain connectivity on sustained attention task performed by children between 7 to 13 years old from a public school. Ten participants were ADHD-diagnosed and five were selected for the control group to compare EEG signals collected with low-cost neuroheadset.

Graphs show different connectivity dynamics in both groups for Theta (4-8 Hz), SMR (12-15 Hz) and Beta (15-20 Hz), indicating connectivity variations in brain regions according to the neuroenergetics theory. The connectivity in the ADHD group is reduced in lower frequencies first (Theta), then SMR and finally Beta. In contrast, the control graphs for Theta and SMR brainwaves are closer to the small-world networks and it can be noticed by comparing the measurements of the different graphs among themselves. The decay process corresponds to the bottom-up approach, where random stimuli trigger transitions from one state to the other, which is in this case the transition from attention to inattention.

The declining of resources placed for disposal at the randomized SART stage might imply a limitation regulating the production of the required resources for the tasks fulfillment, as it has been reported in previous studies where other techniques are implemented.

2 Introduction

Engineering develops designs, models and techniques by means of mathematics and physics for solving the problems of humanity, such as the construction of infrastructure, transportation systems and hydraulic systems. These findings are known as technology.

The greater number of technological advances in the history of humanity are recognized during the Industrial Revolution, a time when the civilization went from a rural economy with low capital available to a technicized society, where the possibility of acquiring goods increased thanks to the incorporation of machines that reduced the requirement of manpower and speeded-up the production times. The industry emerges as the economy basis, giving place to the transition to a new type of social model, thus defining the information and service-oriented society.

As the industrial production was stablished, engineers focused on other necessities for improving the living conditions of the people, like health care. The rate mortality in industrialized societies decreased due to an increased knowledge in every fields, resulting in an enhanced alimentation and sanitary progress. Some of the most significant inventions, regarding to health are the blood transfusion, the x-rays and the antiseptic techniques.

There were some advances health-related using electricity too, such as the electrocardiogram and the electroencephalogram for recording the electrical activity of the heart and the brain, giving the possibility of detecting electrical changes on the skin arising from the respective organ.

Emphasizing on brain, neurocognitive functions and electroencephalography (EEG) were allied for the first time in Hans Berguer "*Über das elektrenkephalogramm des menschen"*[1], characterizing alpha and beta rhythms and recording the first electroencephalogram. Before EEG there were not techniques for measuring the electrical activity of the brain and therefore, indicate the general person consciousness since each state (i.e. wakefulness or dreaming) is related to particular EEG patterns. The electric signals in an EEG are wavy lines with peaks and valleys that with a professional interpretation it can be noticed if there are abnormal patterns in brain activity. Some might occur due disorders or injuries.

The advances in informatics on the Third Industrial Revolution started in 1945, when the state became a heavy funder of R&D. The global scientific leadership shifted from Western Europe to the United States. After war and depression, global trade and investment flows reemerged producing the expansion of international flows of technology [2].

All the findings where enhanced once the processing and the storing capacity in computers became sophisticated enough [3]. It made possible to obtain and analyze big amounts of data in short time, transforming them into information[4]. Brain sciences have taken great advantage due to this integration[5], making possible the appearance of less invasive treatments, biotechnology and earlier diagnosis.

3 Project Definition

The human brain has a larger cerebral cortex than any other animal and utilizes 25% of the total glucose production. Despite it is only a 2% of the completely human body's weight.

Brain neurons input nutrients for signalizing and transmitting information through electro-chemical processes, giving rise to functional connectivity. Due to their expansive dendritic arbors and long-range projecting axons, neurons should maintain the connectivity required for supporting perception, action, language, thinking, social behavior and other neurocognitive functions.

Nowadays, there are many invasive and non-invasive methods for obtaining electroencephalographic (EEG) signals: Invasive methods imply to cut across the skin and place electrodes for sensing electroencephalographic (EEG) activity; on the other hand, for non-invasive methods, there is a wide variety of instruments, going from hoods full of electrodes to single-electrode neuroheadsets. For non-clinical professionals the latter ones are more appropriated.

Once an EEG (invasive or non-invasive) device is selected and the EEG signals are recorded, the real question emerges how to interpret the signals. A strong knowledge is needed for understanding them and what their variations mean, but almost no clinical or non-clinical professional has it due the low and centralized economic resources for neurosciences in Colombia, and the lack of cooperation between engineers and clinicians.

The graphs and their measurements from the small-networks approach bring crucial information allowing a very easy, fast and visual interpretation, and provide a good solution for non-experienced professionals in EEG signals with little time for studying the tendency of the signals.

The proposed methodology utilizes a low-cost portable EEG (costs USD $400 + shipping), an Emotiv Epoc device [6-8]. This device has only 14 electrodes, but still gives the possibility to build 14-node graphs displaying relevant information.

4 Project Justification

Thanks to Resolution 2565 of 2003 [9], public schools must include students with special necessities. In the case of intellectual disabilities and autism, the percentage of integrated students has to be maximum 10% per group, and for motor, visual or auditory disabilities, this percentage have to be less than 40%. On the other hand, expansion does not mean inclusion and that is why even if public institutions must create an academic alternative for these students, there are not enough resources assigned by the Government and limitations prevail.

ADHD (Attention Deficit Hyperactivity Disorder) children are fuzzily included in this resolution, even when previous studies like [10] and [11] have shown an ADHD index is higher in Colombian inhabitants than other populations, making them a crucial target of study for generating solutions.

ADHD is considered a neurodevelopmental disorder according to DSM-V (The Diagnostic and Statistical Manual of Mental Disorders, Fifth Edition) [12], and associated to great risks in low school performance, addictions, depression, aggression, anxiety, and other difficulties in social, academic and working contexts[13].

In Colombia, there are very few EEG options, and the ones available are expensive and/or placed in laboratories. Furthermore, all the equipment has to be imported from USA, Taiwan, Germany… owing to there is not any industry producing them in Latin America and it carries also importation taxes, having most of the EEG devices prices greater than USD $1000 and going to USD $80.000 and more. Some of these devices are not even exported from their home countries, adding an extra impediment.

Health professionals need engineers for assisting them in the use of technology because generally, they are not skilled enough in the use of certain tools or devices, or they do not know what to do with the collected data. On the other hand, engineers are skilled in the use of tools, but usually they are focus more in have a good tool than in the practical use the tool might have.

For these reasons, there is urgency to develop not-pharmacologic low-cost methods using technology for supporting ADHD people and therefore, understand their differences and track their progress assessment and therapy.

As the implementation proposed is very cheap compared to other methods and devices and implies no risk of radiation (as MRI or MEG), it might be the first step for alternative tool for neuroscientists, clinicians and non-clinicians with low-resources to understand ADHD. If additional theories are developed according to this system, other conditions, diseases and disorders related to brain functionality will be studied using the system.

5 Objectives

5.1 Main Objective

To analyze functional connectivity differences between ADHD children and control children using an electroencephalographic low-cost neuroheadset.

5.2 Specific Objectives

- To process the EEG signals into a graph representation of functional connectivity.
- To use a validated statistical method for analyzing the synchronization phenomena in electric signals.
- To establish behavioral and connectivity differences between ADHD children and non-ADHD children through the behavioral responses and the EEG signals.

6 Structural and Functional Connectivity

Structural and functional connectivity are the two main kinds of brain connectivity.

- **Structural Brain Connectivity**

Represents structural associations among different kinds of neural elements, including both morphometric correlation and authentic anatomical connectivity [14-16].

  - **Morphometric correlation:** It is applied relating the different brain regions of MRI structural data and it might be obtained examining the statistical interdependencies of morphologic descriptors *e.g.* the area surface, the cortical thickness or the regional volume of gray matter.
  - **Authentic anatomical connectivity:** It might be obtained examining the white matter fiber connections via diffusion.

- **Functional Brain Connectivity**

Represents the functional associations among the brain regions and might be obtained measuring temporal correlations between spatially remote neurophysiological events and the data acquired using fMRI and EEG/MEG techniques. Once brain connectivity information is extracted from the neuroimaging or signals data, graph theoretical approaches might be applied to brain networks models and analyze their topological subjacent properties [17].

Human cognition is associated to the rapidly changing activation neuron patterns and are vastly distributed, involving numerous cortical and sub-cortical regions activated given different combinations and contexts. Two fundamental and organizational principles of the neural cortex are the functional segregation and the functional integration, allowing a fast data information and the coherent brain states generation [18].

There have been meaningful advancements related to the understanding of the structural properties of networks and their dynamical nature, *e.g.* synchronization capability of the complex networks depicted in coupled oscillators might be determined using graph spectral analysis.

New applications for neurosciences have been inspired using the theory of graph analysis for complex networks. Graph analysis has been implemented for neural networks model, anatomic connectivity and functional connectivity based in fMRI, EEG and MEG. The studies suggest the human brain modeled as a complex network, with appropriate allowance to a small-world structure in both anatomical and functional levels, hypothetically reflecting an optimal situation associated to rapid synchronization and information transference, minimum wiring costs, as well as an equilibrium between local processing and global integration. The topologic structure of functional networks might be restricted by genetic and anatomic factors, but also modified while tasks are being performed. The evidences for mental diseases such as Alzheimer, schizophrenia, brain tumors and epilepsy indicate an existent relation with the optimal small-world pattern deviation of the neural network topology[19].

The neural network topology critically affects the neural signaling and information. Despite the importance of the neural information processing, the cortical networks topology is only partially

understood. There is still extremely vague and rudimentary information about the connectivity matrix in any specie [20], especially the human brain cortex [21].

The augmenting volume of connectional information requires the development of new methods for computational neuroanatomy, including new ways for reunite, store and file connectivity datasets [18].

6.1 Functional Brain Connectivity

In 2010, guided for the connectivity maps potential, the NIH (National Institute of Health) launched to developing technologies that might provide a precise map of mammals' brain in the neural level.

The Human Connectome mapping offers a unique opportunity for understanding the complete details of the neural connectivity [22-24]. The Human Connectome Project (HCP) [25, 26] is a Project for building a full map of the structural and functional neural connections in vivo, inside and outside of them. The HCP presents the first large-scale attempt for gathering and sharing data with enough detail and scope, thus profound fundamental questions are encompassed for analyzing the human connectivity and its variation.

Brain connectivity can refer to different concepts depending on the study, and that is because the connectivity network encodes important information about brain structure and brain functioning.

Talking about structural connectivity, physical connections through synaptic contacts communicate distant brain regions. These connections are fiber tracts called white matter, consisting mostly of glial cells and myelinated axons. The set of connections is visualized using data collected by Diffusion Tensor Imaging and then a 3D model is obtained thanks to the tractography technique [27-29].

In functional connectivity, similar patterns of brain activity among different brain regions are detected. Neurons are connected to other neurons generating synaptic activity, where each synaptic impulse is an electrochemical signal generated primarily via the activation of voltage-gated calcium channels placed along the cell membrane.

Synaptic activity can be detected using functional magnetic resonance imaging (fMRI) but also in electroencephalography (EEG). Both excitatory postsynaptic potentials and inhibitory postsynaptic potentials contribute to the synaptic activity recorded as EEG. Scalp electrodes record potential differences generated by postsynaptic potentials in the cell membrane of cortical neurons [30].

The signals collected by the electrodes are statistically analyzed pair-by-pair as temporal dependencies of neural activation patterns. The statistical measure utilized could be correlation, phase locking, synchronization or spectral coherence. The statistical values obtained for each pair of EEG signals are the input for the functional-connectivity matrix.

6.2 Graph Theory

Graph theory (GP) is a useful tool for analyzing brain connectivity [31]. The nodes are represented by electrodes placed on the scalp or brain regions (if there are neuroimaging techniques involved), and the edges are the relations among them using i.e. synchronization, coherence or correlation measurements[14]. Its applications vary depending on the research approach [32], permitting an easier and faster understanding of the results obtained compared to other methods.

GP has been used for characterizing different brain-related diseases and disorders i.e. Alzheimer [33-35], epilepsy [35-37] and Parkinson [38, 39] from the structural and the functional perspectives. From the structural perspective the physical connections are identified among the regions of the brain, from the functional perspective the synaptic ones are the relevant connections.

In recent years, some theories have been developed for explaining attention from the neurobiological substrates, but there is still no evidence of how mind-wandering states are visualized in terms of connectivity nor the changes on a patient subjected to therapy.

There are different techniques for sensing brain activity, going from imaging techniques to functional techniques like EEG (see Figure 6.1). EEG is the most acceptable technique for analyzing global functional connectivity related to cognitive tasks in real time for its low spatial resolution, which is compensated with its high temporal resolution [40].

EEG data should be compared with the data obtained using another process. For measuring the participants' evolution, the signals studied through graph theory are contrasted with the results of a paradigm for sustained attention.

For study attention, there are several biomarkers such as the theta/beta ratio approved by the FDA or synchronization and phase measurements [41-43] like Phase Lag Index (PLI), Phase-Locking Value (PLV) and Synchronization Likelihood (SL). A biomarker is a biological measure that senses objectively a biological process, helping to predict health states and thanks to them, know if an intervention is working or if there are differences in different subjects or groups of people.

These biomarkers can be found using a neuroheadset. The neuroheadset is an Emotiv Epoc, a low cost peripheral with only 14 electrodes designed mainly for recreational purposes, but also useful for research purposes [8, 44, 45].

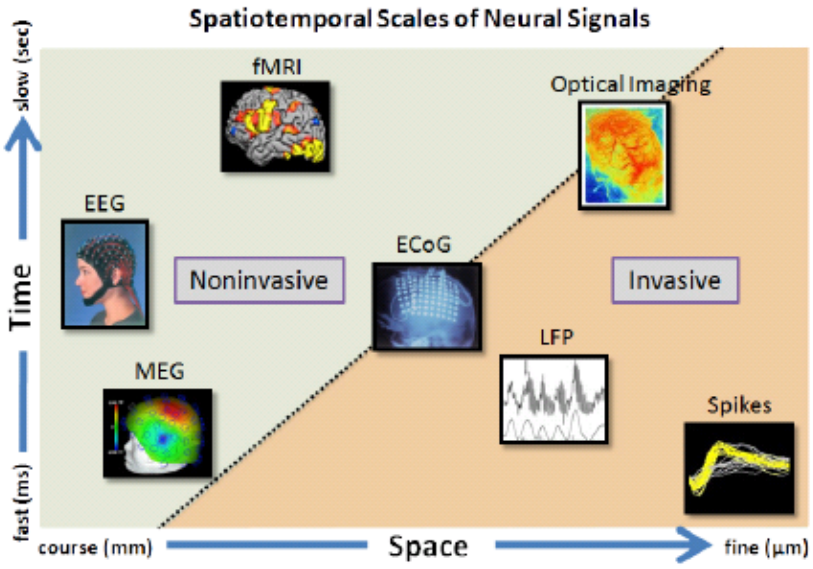

Figure 6.1. Rendering of different signals from the brain potentially usable for brain machine interface. The graphic illustrates the temporal and spatial scales for each signal. Courtesy of: [46].

6.3 Network Properties

Stam *et al.* [32] proposed a simple definition for small-network properties, very close to the one proposed by Onnela *et al.* [47] but adding the symmetry concept for an edge w connected to nodes i and j ($w_{ij} = w_{ji}$) and maintaining $0 \leq w_{ij} \leq 1$.

Degree (k): Equals to the number of links connected to a node, which is also equal to the number of neighbors of the node, as it is shown in 6.1.

$$k_i = \sum_{j \in N} a_{ij} \qquad 6.1$$

Where
N is the set of all the nodes in the network.
n is the number of nodes.
(i, j) is a link between nodes i and j, $(i, j \in N)$.
a_{ij} is the connection status between i y j: $a_{ij} = 1$ when link (i, j) exists (when i and j are neighbors); $a_{ij} = 0$ otherwise ($a_{ij} = 0$ for all i).

• **Number of triangles (t)**: It is a basic measure of integration that returns the number of triangles around a node i, as it is shown in 6.2.

$$t_i = \frac{1}{2}\sum_{j,h\in N} a_{ij}a_{ih}a_{jh} \quad 6.2$$

• **Clustering coefficient (C):** The weighted clustering coefficient is defined as a real number between 0 and 1, where 0 represents no clustering and 1 maximal clustering [48]. The average clustering coefficient for a network is defined as 6.3 and 6.4:

$$C = \frac{1}{n}\sum_{i\in N} C_i \quad 6.3$$

Where

$$C = \frac{1}{n}\sum_{i\in N} \frac{2t_i}{k_i(k_i-1)} \quad 6.4$$

• **Characteristic path length (L):** It is always positive because the weight link is calculated using a phase synchronization measure, in this case Phase Locking Value (PLV).

It is the average shortest path length between every pair of nodes in the network. A trajectory length is weighted between two nodes, and defined as the sum of the nodes length for this trajectory. The shortest trajectory l_{ij} between two nodes i and j is the trajectory between i and j with the shortest length. Similarly to 6.3, the average weighted length of the trajectory for the whole graph is calculated with 6.5 and 6.6:

$$L = \frac{1}{n}\sum_{i\in N} L_i \quad 6.5$$

Where

$$L_i = \frac{1}{n}\sum_{i\in N} \frac{\sum_{j\in N, j\neq i} d_{ij}}{n-1} \quad 6.6$$

• **Global efficiency (E):** It is the average of the inverse shortest path length and is inversely related to the characteristic path length. Unlike L, E might meaningful computed on disconnected networks as paths between disconnected nodes are defined to have infinite length, and correspondingly zero efficiency [32]. It is a measure of how efficiently a network exchanges information [49] according to 6.7 and 6.8.

$$E = \frac{1}{n}\sum_{i\in N} E_i \quad 6.7$$

Where

$$E = \frac{1}{n}\sum_{i\in N}\frac{\sum_{j\in N, j\neq i} d_{ij}^{-1}}{n-1} \quad 6.8$$

- **Local efficiency:** It is the global efficiency computed on node neighborhoods, and it is related to the clustering coefficient. It is calculated from the efficiency of connections between first-degree networks of each node [50], as in 6.9 and 6.10:

$$E_{loc} = \frac{1}{n}\sum_{i\in N} E_{loc,i} \quad 6.9$$

Where

$$E_{loc} = \frac{1}{n}\sum_{i\in N}\frac{\sum_{j,h\in N, j\neq i} a_{ij}a_{ih}\left[d_{jh}(N_i)\right]^{-1}}{k_i(k_i-1)} \quad 6.10$$

6.4 Small-World Problem

The easiest way for starting with the small-world problem is starting with each pair of people in the world. What is the probability that they know each other? According to Milgram [51], there is a more sophisticated formulation, however, it considers the fact that while people X and Z might not know each other directly, they could be related to a unique same person. There is the possibility of a chain relation with X knowing Y and Y knowing Z. Besides, it is possible to imagine circunstances where X is connected to Z but not for an only link, but for a series of them: $X - a - b - c - \cdots y - Z$. It means that the person X knows the person a, who knows the person b, who knows the person c… who knows the person y, who knows the person Z.

Thus, another question emerges: *Given any two people in the world, person X and person Z, how many intermediate-links relations are needed before X and Z are connected?*

6.4.1 Why We Should Perceive the World as a Small-World Phenomenon?

There are four criteria needed for making the small-world phenomenon memorable:

- The network is numerically big in the sense that the world contains $n \gg 1$ people. In the real world, n is in the order of thousands of millions.
- The network is sparse in the way that every person is connected to an average of another k people, which is at least in the order of thousands [52], thousands of millions less times than the planet population.

- The network is decentralized. Then there is not any dominant vertex to which most of the vertices are directly connected. It implies a more important condition than the shortage: not only the average grade k should be less than n, but the maximum grade k_{max} above every vertex should be less lower than n.
- The network is highly clustered when most of the friendly circles are strongly overlaid. That is to say, it is expected that many of our friends are friends with each other.

If the world does not have many people, then it should not be shocking that every people are tightly associated (like in a small town). If most of the people know the vast majority of people, then again it would not be surprising that two strangers know each other. If the network is highly centralized –like a star-, then a short trajectory might exist between your center and every pair of vertices.

If the network is not clustered –*i.e.* if every person chooses their friends independently to their friends' choices- it will follow the random graph theory [53], where most of the people will be just a few degrees of separation even for huge n values, but are these criteria satisfied in the real world? Being the world population of thousands of millions and being generous estimating how many familiar people may someone have, it is possible to say that an average person might have only a few thousands of knowns, fulfilling the first two criteria.

The last two criteria are more difficult to guarantee and are certainly harder to measure even when are reasonable from the everydayness perspective.

6.5 Graph Theory and Small-World Networks

Graph theory is a formal representation of networks. Graphs comprise two elements: (1) nodes or vertices, representing the elements in the study and (2) edges, representing the relations among the elements. In the context of neuroheadsets, the nodes are electrodes and the edges are synchronizations among the signals generated. Small-world properties such as clustering coefficient and characteristic path length are measured and its relation determines how ordered or disordered a network is [17, 54, 55].

Recently, graph theory has attracted considerable attention to the brain networks researchers for the powerful way it quantitatively describes the topological organization of brain connectivity. According to the theory, the brain might be represented as composed graphs of nodes representing electrodes, regions or voxels, and the edges represent structural or functional connectivity [17].

6.5.1 Types of Networks:

In [56], the authors proposed an algorithm for explaining the interpolation between regular and random networks using a random rewiring procedure. Starting with a lattice ordered network, with probability p a link is reconnected to a randomly chosen vertex. If a network is totally ordered or lattice, then it has a probability of rewiring of $p = 0$, but as long as p is getting approached to 1, the network is going to be more random. The small-world networks

arise in the middle of ordered and random networks, and they compound the high clustering coefficient of ordered networks and the characteristic path length of random networks.

The three basic network measures are depicted in Figure 6.2 according to the model of Watts and Strogatz [56] and described below:

- **Ordered or lattice:** This network has a high clustering coefficient C and a long path length L. The degree of every node in the network is the same because every node is connected to its k neighbours.

- **Small world:** It is characterized for a high C and a low L, making it effective. It is an ordered network with few randomly rewired links and regarding that most nodes can be reached from every other node by few steps. Thus, small-world networks introduce the concept of hub node, a better-connected node that reduces dramatically the distance among the other nodes in the network.

- **Random:** The C and L are low. A random network is the opposite of an ordered network due to the way its links are connected is completely random. These networks have the particularity that the information travels easy but if any link is lost, the network will possibly be vulnerable.

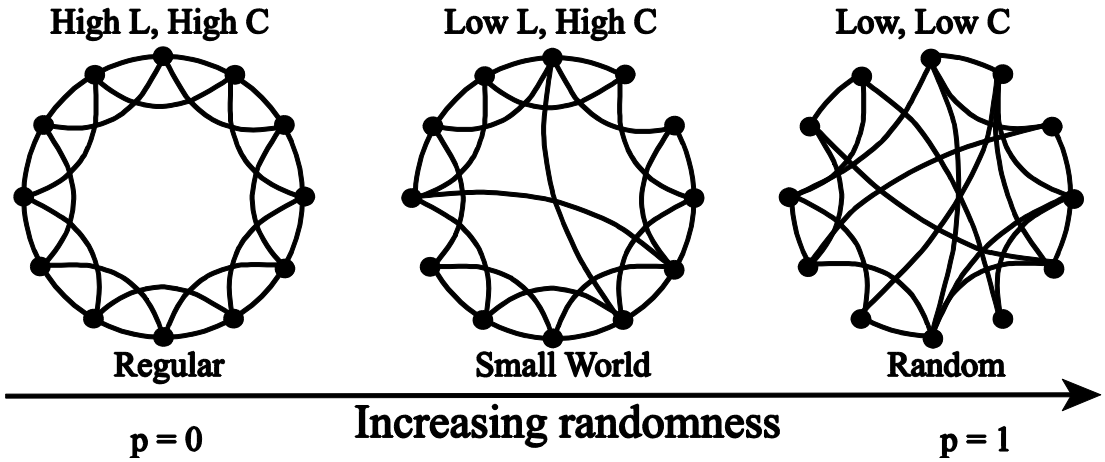

Figure 6.2. Three basic network types in the model of Watts and Strogatz [56]. The three networks have 16 vertices (N=16).

6.6 Small-world Networks in Neuroscience

Small-world networks are optimal, allowing an efficient information processing using a minimum connection links. Here to fore, it has been proven that many types of networks, going from metabolic and genetics to social networks, are small-world networks [57, 58].

As Bassett and Bullmore [15] have exposed before, there are theoretical and experimental reasons explaining beforehand why small-networks present an attractive model for brain network connectivity:

- The brain is a complex network with multiple time and spatial scales. This fact alone might motivate a small-world analysis for brain networks, given the extensive occurrence of small-world properties in many other complex networks through a physic scale manifold.
- The brain supports the processing of both types of information: distributed and segregated. The network architecture is considered a key substrate for sensorimotor and cognitive processes, which might be discretely located in specialized regions or represented by coherent oscillations in large-scale distributed systems.
- The brain evolved possibly for maximizing the efficiency and/or minimizing the information processing costs. The small-network topology is associated to global and local efficiency of parallel information processing, sparse connectivity and low wiring costs. Small-world networks are able to operate dynamically in critical states, facilitating the fast and adaptive resetting of the formations supporting the cognitive states changes.

Since the discovery of small world networks, the study of complex systems from the networks perspective has obtained recognition and in the recent years, many important properties have been traced [31].

For structuring brain connectivity as something so difficult, a historical revision is necessary. During the last century, brain researches have been appointed for a peculiar dichotomy: while many neuro-anatomists work diligently testing how different neuronal populations are connected to each other with the purpose of constitute networks, neurophysiologists are usually forced to register a neuron or neuronal assembly at the time, focus on try to determine the functional specialization of the register unity. This emphasis was introduced by neuropsychology, routing behavioral consequences of localized brain seizures [59]. Thenceforth, the modular specialization or function became the predominant paradigm for what we call at present cognitive neuroscience (e.g. [60]).

Nevertheless, for each technique utilized for obtaining neurophysiological data, there are always some researches trying to obtain their data from two or more neuronal elements –or from two or more brain locations- simultaneously, or interpreting the data of neuronal interactivity. However, the way it has been achieved involves the evaluation of some kind of covariance or correlation among the multiple signals registered. An amount of more complicated measurements, going further the simple correlation, have been utilized on these studies (e.g. regression analysis, principal components analysis and multidimensional adjustment), But in a conceptual level, all this methods include the covariation notion along the activities.

6.7 Techniques

There are two kinds of techniques:

6.7.1 Extraction

- **fMRI (Functional Magnetic Resonance Imaging):** Graph theory might be utilized as a new approach to identify the functional clusterization in activated brain areas during a task. Initiating the brain activity BOLD (Blood Oxygenation Level Dependent), a correlation

matrix among the time series is computed, and the matrix become a graph (undirected and unweighted) assigning the edges to all the suprathreshold correlations. From this perspective, it is possible to show different functional clusterizations as subgraphs *i.e.* while a typing task is performed. The threshold has a pivotal influence in the results and the criterion for choosing am optimal threshold has to be taken very seriously.

- **EEG/MEG (electroencephalography/magnetoencephalography):** When brain networks are considered, the network edges ideally represent significate brain regions. The use of EEG/MEG sensors as edges is a common practice, but such results have to be carefully interpreted as the electromagnetic signals are collected due to its propensity to spatial superposition.

  Regarding the network links, these might represent functional or structural associations. In the structural networks, the links should represent anatomical connections between brain regions, and the different weights might represent the fiber tracks size, quantity or coherence. For functional and effective networks, the links represent some correlation measurements or casual influence respectively, among the connected edges activity [32, 61].

6.7.2 Analysis

- **Phase lag index (PLI):** It is an asymmetry measure of the difference-phase distribution between two signals. PLI reflects the consistency between which signal is in the main phase or in the lag phase with regard to the other signal. PLI [19] performs at least as well as the probability of synchronization [62] detecting real changes in synchronization, but it is less affected by simple sources influence.

  Besides the global-weighted PLI computation, it is possible to use a more regional approximation. The MEG sensors might be clustered in 5 different regions: frontal, temporal, central, parietal, and occipital. An average PLI might be also calculated for all the sensors inside a region or between two regions (a long distance).

6.8 Some Problems Studied using these Techniques

A good amount of studies have study the nature of networks shifting in different kinds of brain pathologies. In the case of brain tumors, schizophrenia and interictal recordings of patients with pathological epileptic networks, characterized by smaller C and L [36, 63, 64].

Considering Watts and Strogatz model, where in a highly ordered network with grade K are rewired randomly with a probability of certainly P, some smaller C and L might correspond to a higher rewiring probability value, and a more randomized network [19].

6.8.1 Schizophrenia

The cognitive dysfunction is seen as the core of schizophrenia, a chronical psychotic disorder. The fMRI researches reveal abnormal brain activity in patients with schizophrenia during cognitive tasks involving language, memory and attention. The functional brain

disconnectivity has been considered the symbol of schizophrenia. Recently, the brain activity exploration in absence of specific emotional or cognitive tasks has been the center of fMRI researches.

The aberrant steady-state have been one of the more robust schizophrenia biomarkers, revealed often in the independent component analysis (ICA). ICA was developed for solving problems similar to the "cocktail party" scenario, applied to fMRI data determining a set of brain networks. The interrelation between many maximum neuronal networks especially independent where each one of them has time courses associated. This approaching is very useful for examining the cerebral activity during functional connectivity states between the time courses of ICA data components collected from fMRI steady states.

The interrelations between multiple brain networks, also known as components, were definite as a functional network connectivity. Yu et al. [65] examined the differences between control subjects and schizophrenia patients and many other higher correlation occurrences among the schizophrenia patients' networks. However, the topological properties of the connectivity relations in functional networks have not been studied yet.

6.8.2 Alzheimer

The large-scale structural changes in brain networks were examined in the steady state of Alzheimer patients compared to non-demential patients using graph-theory concepts. The MEG were recorded in 18 Alzheimer patients and 18 non-demential control subjects in a state were no task must be accomplished and their eyes were closed. For the main-bands frequencies, the synchronization between every MEG pair of channels was evaluated using a PLI (Phase-Locking Index), an intensive synchronization measure for the conduction volume. The weighted networks were calculated and characterized using a clustering coefficient and a trajectory length. The Alzheimer patients evidenced a medium PLI decreasing in the beta and lower alpha bands. In the lower alpha band, the clustering coefficient and the trajectory lengths decreased in Alzheimer patients. The network modifications for lower alpha might be explained better using a "Targeted Attack" model [66] instead of a "Random Failure" model [67]. In this way, Alzheimer patients show a lack of functional connectivity in a resting state for beta and lower alpha bands, even when a non-sensitive measurement is utilized for volume conduction effects. Besides, in the lower alpha band, the functional networks big-scale structure is more randomized in Alzheimer patients, thus the modeling results suggest that in the neural network, the highly connected hubs might be at risk.

Stam and Reijneveld [68] findings in the Alzheimer group occur as C and L decrease, and a more randomized network. Furthermore, the values are closer to one, indicating that the difference between real and random networks is too small. The only finding that does not fit among the other findings is the trajectory length increment in Alzheimer patients' beta bands reported by Stam *et al.* [69] in a previously reported pilot study. This result was obtained just for some Kvalues, using an identical K value for both groups. An explanation might be that the unconnected points reduce or augment the trajectory length considerably.

7 EEG Signals

Electroencephalography is a neurophysiological exploration that records the bioelectrical activity along the scalp offering one of the best quality-price benefits and its fabrication is simple.

Resulting from small ionic currents produced when a population of synchronized neurons fire. The information travelling via electric impulses is received from other neurons in the dendrites and pass through the neuron until it is driven by the axon to the this is the electrochemical signaling sensed by electrodes placed on the scalp, obtaining as EEG signals as number of electrodes (discarding the reference electrodes) the EEG device has.

These electrical activities from the brain, called brainwaves, are represented as waveforms of varying frequency and amplitude measured in microvolts. Brainwaves emit tiny electrochemical impulses classified according to its frequency in:

- **Delta (0-4 Hz):** It is the slowest frequency, experienced in non-awareness. The Delta is rhythm emerges during very deep transcendental meditation and dreamless deep sleep. Abnormal Delta activity may evidence learning disabilities, difficulties for being conscious aware if any brain injury exists and severe ADHD.
- **Theta (4-8 Hz):** It is experienced during meditation, creative states, REM sleep and peak experiences. Abnormal Theta activity may evidence ADHD, inattentiveness, hyperactivity, impulsivity and depression.
- **Alpha (8-12 Hz):** It is experienced during all-senses visualization or relaxation states. Abnormal Alpha activity may evidence difficulty to focus and a lot of relaxation.
- **Beta (12-30 Hz):** It is experienced during the awareness state, outward attention and analytical thinking. Abnormal Beta activity may evidence anxiety, inability to relax, panic, stress or high arousal.
- **Gamma (> 30 Hz):** Gamma waves are difficult to detect. It is experienced during cognitive functioning and higher processing tasks. Abnormal Gamma activity may evidence high arousal, stress and anxiety.

EEG counts with the advantage of having high temporal resolution in the order of milliseconds but the spatial resolution is however, of the order of centimeters and not millimeters. It is a non-invasive technique which allows the estimation of the underlying electric sources of the brain [70]. This mechanism can be applied to study the dynamics of networks with high temporal resolution, enhancing our knowledge on neurophysiological substrates of behavioral disorders.

7.1 Signal Filtering

A Finite Impulse Response (FIR) filter is utilized instead an Infinite Impulse Response (IIR) filter because FIR filters filter the signal in time domain and IIR filters in the frequency domain.

The correct number of coefficients, also known as the order of the filter, for setting up an FIR filter is determined by a rule of thumb, where the number of coefficients should be equal or greater to four times the sampling rate divided by the lower edge frequency. The FIR filter approaches to the ideal filter as the filter order increases, but at the same time the complexity and amount of time for processing input samples is increased.

7.2 Hilbert Transformation

The Hilbert Transform (HT) is a linear operator useful for analyzing nonstationary signals. It is possible by expressing the frequency as a rate of change in phase, making the frequency vary with time.

Through the construction of the analytic signal, the Hilbert transformation (see Figure 7.1) gives the instantaneous phase for a signal, where the instantaneous phase is formulated as in 7.1

$$\phi(t) = \arctan\left(\frac{s_H(t)}{s(t)}\right). \quad 7.1$$

The Hilbert transform is useful for analyzing nonstationary signals by expressing frequency as a rate of change in phase, so the frequency is able to vary with time. According to Pikovsky, Rosenblum and Kurths [71], the analytic signal is expressed as in 7.2

$$\zeta(t) = s(t) + is_H(t) = A(t)e^{i\phi(t)}. \quad 7.2$$

The analytic signal comprises the original signal and its Hilbert transform. The instantaneous amplitude obtained from the analytic signal is $A(t)$, the instantaneous phase is $\phi(t)$, and $s_H(t)$ is the Hilbert transform of the signal $s(t)$ as in 7.3

$$s_H(t) = \frac{1}{\pi} p.v. \int_{-\infty}^{+\infty} \frac{s(\tau)}{t-\tau} d\tau \quad 7.3$$

The application of the convolution theorem turns the equation into 7.4

$$s_H(t) = -FT^{-i}\left[FT[s(t)]sign(\omega)\right] \quad 7.4$$

Where FT denotes the Fourier transformation and FT^{-1} denotes the inverse Fourier transformation.

The instantaneous phase of the Hilbert transformation is limited to $[0,2\pi]$ and is unwrapped before taking its derivative.

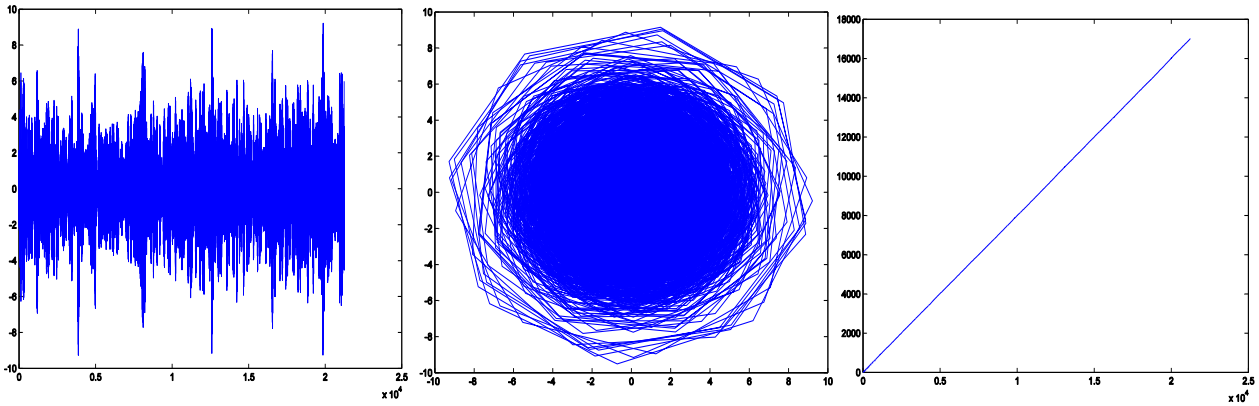

Figure 7.1. Left: The original signal $s(t)$ collected from an electrode. Center: Hilbert transformation of the signal $s_H(t)$. Right: Instantaneous phase of the Hilbert transformation $\phi(t)$.

If a signal is filtered in a particular band, then the data is forced to assume a sinusoidal oscillating state. Once it is filtered, it is possible to calculate the instantaneous phase at any given time point along the discrete signal.

The further advantage of the HT is the sensitive access it gives to amplitude patterns of analytic amplitude that are correlated with intentional behaviors [72].

The HT is an efficient and quick tool for extracting the phase values, and the Phase-Locking Value technique was initially formulated with this transform.

7.3 Phase-Locking Value

Synchronization is known as the rhythmic adjustment of self-sustained periodic generated by a weak interaction between them [73]. This phenomenon of adjustment is described as phase locking and frequency entrainment. Synchronization is widely explored in rotators, chaotic systems and studies of nonlinear dynamics systems. It is also widely incorporated in the modeling of biological systems demonstrating oscillating behavior, like physiological systems [74].

Phase-Locking value (PLV) is a statistical method for studying the synchronization phenomena measuring synchronized activation over different brain regions. The phase differences are utilized for analyze biological time series (irregular, non-stationary, non-linear and noisy) of the brain electrical activities. Its detection can provide an indication of short-range synchronies, commonly interpreted as subserving "perceptual binding" among adjacent or same brain regions. More interesting, it can describe long-range synchronization patterns between widely separated brain regions, thought to subserve cognitive mechanisms, such as memory, emotion and motor planning.

PLV measures the synchronization between all electrode pairs, similarly to the cross spectrum technique. As 7.5 indicates, N represents the total number of trials, $\Delta\Phi(t,n)$ is $\phi_a(t,n) - \phi_b(t,n)$, the phase difference between two signals a and b, and t is the time of each period [75].

$$\varphi(t) = \phi_a(t) - \phi_b(t) = \arctan \frac{s_{H_a}(t)s_b(t) - s_a(t)s_{H_b}(t)}{s_a(t)s_b(t) + s_{H_a}(t)s_{H_b}(t)} \quad 7.5$$

Then, for finding the synchronization between two signals obtained from the same subject, the mean phase coherence of an angular distribution is computed using 7.6

$$R = \left| \frac{1}{N} \sum_{j=0}^{N-1} e^{i\varphi(j\Delta t)} \right| = 1 - CV \quad 7.6$$

Where $\frac{1}{\Delta t}$ is the sampling rate of the discrete time and CV is the circular variance of an angular distribution obtained after transforming the relative phase angles onto the unit circle in the complex plane [76].

The R value is going to be considered from this point as the Phase Locking Value (PLV).

7.4 Graph Construction

The PLV value for each pair of signals is a number between 0 and 1, where 1 represents that one signal is perfectly following the other and 0 means that they are not associated at all. As the main interest is to understand how connectivity works in the children's brains while performing the tasks, average graphs are constructed. The code developed in MATLAB for visualization can be found in Appendix C.

The graphic interface was developed on MATLAB and based on the BCT toolbox measurements [32].

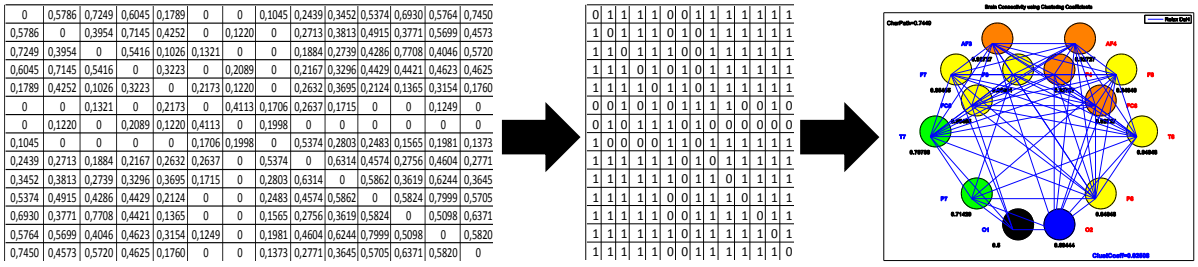

Figure 7.2. Left: Weighted connectivity matrix. Center: Binarized connectivity matrix. Right: Resulting graph.

As it is shown in Figure 7.2, after the weighted connectivity matrix is obtained, a threshold must be selected very carefully. According to the threshold, the matrix is filtered. The link values below the threshold are turned into zero and only those links representing the functional connectivity are the ones that remain in the matrix. Then, each remaining value is converted into 1, and the network properties are calculated from the binarized matrix.

With the aim of an intuitive visual interpretation, the electrodes have been placed according to the Emotiv Epoc disposition. The local efficiency value obtained for each channel, so the bigger the local efficiency value the bigger the circumference representing the electrode is. A color convention for the local efficiency value is also considered as it is shown in 7.7:

$$color(G_i) = \begin{cases} red, if\ E(G_i) = 1, \\ orange, if\ E(G_i) \geq 0.95, \\ yellow, if\ E(G_i) \geq 0.90, \\ green, if\ E(G_i) \geq 0.85, \\ blue, if\ E(G_i) \geq 0.80, \\ black, otherwise \end{cases} \quad 7.7$$

8 Psychological Test

8.1 Neuroenergetics Theory (NeT)

Neuroenergetic Theory (NeT) states that some psychiatric disorder may occur due to unstable functioning in the neurons feeding chain. Specifically, for Attention Deficit Hyperactivity disorder (ADHD), it might be associated to hypocatecholamine function in subcortical and prefrontal cortical regions, regulated by cortical astrocytes. Astrocyte catecholamine receptors normally regulate energy availability during neuronal activation. Some forms of ADHD may be viewed as cortical energy-deficit syndromes, secondary to catecholamine-mediated hypofunctionality of astrocyte glucose and glycogen metabolism, providing activity-dependent energy to cortical neurons [77].

Recently, Killeen [78] has proposed an examination of this energy misbalance in neuronal circuits through an interactional model among neurons and glia. The most important function of neurons is the synapsis, the transmission of electrochemical information from one cell to another. This process spends energy, major parts of the energy budget are postsynaptic processing and propagation of action potentials, and both are an increasing functions of the stimulation frequency.

Some tasks lead to sustained synapsis in circuit of neurons, the human brain requires to process information continuously and in some cases, long lasting computational effort is required over the same event; after several seconds of firing the neuron relies on lactate provided by the astrocyte in the ANLS. Killeen's hypothesis arguments that in ADHD the cost of transmission for action potentials (c) might be increased, or the rate of supply of lactate (s) might be compromised.

Neurons are not able to produce their own energy, their mitochondria depend of glia cells (astrocytes) functioning, which extract glucose from sanguine vessels to produce lactate. Lactate is diffused into the extracellular space, to be absorbed by the neuron for ATP production, for the posterior restoration of ionic gradients and encapsulation of neurotransmitters. Neurotransmitters and ionic channels are responsible of the electric discharge (potential action) in synapsis.

Glutamate is also converted into glutamine by the astrocytes (See Figure 1), which is shuttled to the neurons to restore their pools of neurotransmitters (yellow arrows). Glutamate, acting on AMPA receptors, stimulates norepinephrine release (red circles) from nearby noradrenergic varicosities. It acts on adrenoceptors, to further stimulate glucose uptake and glycolysis, causing astrocytes produce more lactate to support sustained neural firing.

If astrocytes functioning fail by glutamate action or glucose uptake, the lactate provision for neurons will be compromised. Thereby, neurons will reduce their connectivity and the whole brain would not be able to sustain a continuous computation to response properly to lasting task in the environment. This is the so-called energy misbalance in the neural circuit.

In this stage of low activation, the mind wandering states appear. This concept refers to the occurrence of task-unrelated and stimulus-independent thoughts [78, 79], a fundamental characteristic of inattentive states. It means that the thoughts do not remain on a single topic for a long time and it happens more frequently while an attention-demanding task is performed.

Therefore, there is a clear correspondence between neurons circuits functioning and connectivity with psychological events. Furthermore, the brain's hypoarousal might be indicated by electroencephalography (EEG), short EEG segments have been used to asses vigilance stages, which are corresponding to different states of global brain function [80].

The EEG segments are compared using likelihood measurements for get a probability of how related are the different regions on the brain in the task-related thoughts. From the resulting matrix a graph is constructed and its properties are studied for analyze the network organization.

8.2 Sustained Attention to Response Task (SART)

This test is widely used in psychology for studying attention in people [81] and has been employed in several age groups for studies in different diseases and disorders and has different adaptations.

As this study is directed to ADHD, the adaptation of Johnson et. al. [82] is selected. This adaptation includes three additional masks and different times for displaying each one of them, including the cue.

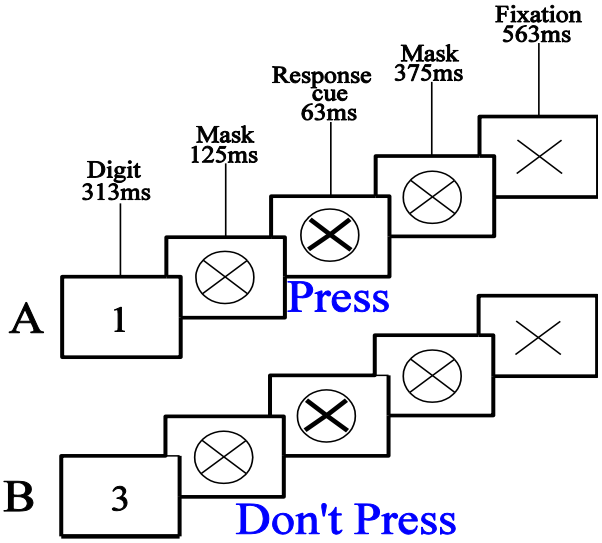

Figure 8.1. SART paradigm modified for ADHD and autistic children according to the work of K. Johnson et al. [82].

In this test, numbers from 1 to 9 are presented in the screen one by time. As Figure 7.1 shows, the digit appears for 313 ms, then a mask for 125 ms, after that a bold mask for 63 ms, again the mask for 375 ms is displayed and finally a fixation mark for 563 ms. The participant has to press the space

bar when they see numbers from 1 to 9, except when 3 is displayed because no key is supposed to be pressed.

The SART of Inquisit Millisecond Software [83] is adapted according to these settings, including all the extra masks and modifying the times for each cue.
The responses are classified in 5 different categories:

(a) ambiguous: it is not clear if the response is anticipatory or successful;
(b) anticipatory: the key is pressed before the digit is seen;
(c) fail: the key is pressed when it is not supposed to be pressed;
(d) omission: the key is not pressed when it has to be pressed, and
(e) success: the key is pressed or not pressed in the right moment.

(a), (b), (c) and are type Go trials and (d) and (e) are type No-Go trials. This information is summarized in Table 8.1.

Category of the response	**Type of response**	**Description**
Ambiguous	Go trial	It is not clear if it is anticipatory or successful
Anticipatory	Go trial	The key is pressed before the digit is seen
Fail	Go trial	The key is pressed when it is not supposed to be pressed
Omission	No-go trial	The key is not pressed when it has to be pressed
Success	Go/No-go trial	The key is pressed or not pressed in the right moment

Table 8.1. Description of the different responses in SART.

8.3 Neuroenergetics Model of Maintained Attention (NEMA)

A Markov model by Killeen [84] is constructed with these responses for understand how the attention-inattention transition works for every group. Killeen reported a slowing and increasing neural in randomized blocks through the SART session.

The author proposed the inclusion of the separate processes of attentional lapses; it has been named the Neuroenergetics of Maintained Attention (NEMA) model, and describes two different contexts: Stimulus-driven recapture and goal-driven recapture. In the first case, involving experimental procedures with conspicuous stimuli, set the probability of recovering attention (α; alpha) to 0 until a target presentation, and thereafter to a value close to 1.

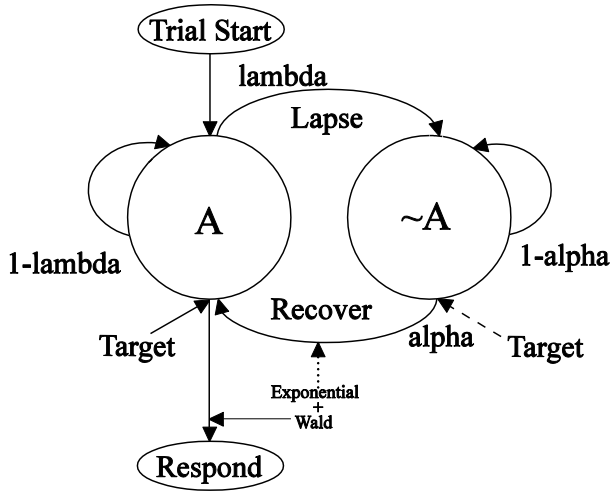

Figure 8.2. The Neuroenergetics of Mantained Attention (NEMA) model.

In this model, Killeen proposed a "double" exponential process to lapse attention as the trials passes and to predict the delay to recapture attentional focus. The author proposes his Markov model for attention from a 2x2 transition matrix. The model follow the representation from Wiener diffusion process for times responses. The data distributions for error or successes are named Wald an Ex-Gaussian distribution. For simple two-choice decisions, empirical RT distributions for humans are generally positively skewed. Increases in the difficulty of a decision lead to increases in mean RT and decreases in accuracy. Increases in difficulty also produce regular changes in RT distributions, changes in their spread but very little change in their shape.

```
*** INPUT ***

  lat 2
        man 4
        dim 2 2 5 2 2 5
        lab X Y P  S T R
  mod
  X|ST
  Y|X
  R|X
     add .05
    dat [12      8       0       8       71
         0       0       1       0       12
         22      14      0       14      49
         0       0       2       0       11
         16      5       0       2       76
         0       0       3       0       10
         2       1       0       80      16
         0       0       1       0       12
         2       4       0       16      77
         0       0       0       0       13
         4       0       0       13      83
         0       0       9       0       4
         4       1       0       9       86
         0       0       8       0       5
         19      5       0       6       70
         0       0       12      0       1
         3       2       0       64      31
         0       0       5       0       8
         0       0       0       69      31
         0       0       6       0       7]

    dum  1 1 1 1 1 1
```
Figure 8.3. LEM code example using the formulated Markov model.

It was intended to fit the NEMA for behavioral data in SART with ADHD and control children; it was calculated the latent class model with two latent variables denoted by X and Y, within the specific path proposed by Killeen, corresponding to attentional and mind wandering states, each one of them having two states. Also, some observed variables were considered and measured through SART: the responses type, trial type, stages and the intra-subject variability.

The Markov model was coded in LEM [85], and an example is given in Figure 8.3.

There are two latent variables: inattention and attention, and four manifest variables: participant, stage, trial and response. The classification of the manifest variables is given in Table 8.2.

Manifest Variable	**Dimensions of the variable**
Participant	As many as participants are
Stage	Fixed SART and randomized SART
Trial	Go or No-go
Response	Ambiguous, anticipatory, omission, failure, success

Table 8.2. Manifest variables and its respective dimensions.

9 Procedure

9.1 Participants

A population of 10 ADHD children and 5 non-ADHD children in ages from 6 to 12 years old will be selected according to the DSM-V criteria. All the participants are students of a public school located in Pereira, Colombia. The data was recorded in each child separately and during the scholar day. The parents signed an informed consent.

9.2 Apparatus

During the whole procedure, every child utilized the Emotiv Epoc neuroheadset, a low cost EEG device created as a peripheral for gaming but also utilized as a researching tool [86, 87].

It is based on the International 10-20 system and has 14+2 channels: AF3, AF4, F3, F4, F7, F8, FC5, FC6, P7, P8, T7, T8, O1 and O2, plus the references P3 (CMS) and P4 (DRL). The letters naming each electrode corresponds to the area of the brain was those have to be placed, as it is shown in Table 9.1.

Electrode	Lobe
AF	Anterior-frontal
F	Frontal
FC	Fronto-central
P	Parietal
T	Temporal
O	Occipital

Table 9.1. The electrodes names and their correspondence to a certain region in the brain.

This device have wireless transmission, making heavy filtering from the oversampling at 2048 Hz per channel to a final sampling rate of 128 Hz, with a frequency response of 0.16-43 Hz.

Figure 9.1. Emotiv Epoc (left) and positioning for each electrode (right).

The children were sited back to a cushion and used an Emotiv Epoc neuroheadset during the whole procedure for recording the totality of the signals. They had a tea table in front of them for perform the test in a laptop. Another laptop was utilized for monitoring the EEG signals collected from their scalps.

9.3 Protocol

The experiment was designed in such way that the child had a more demanding task than the previous one while the time passes by. Before meeting the children, there was a meeting with their parents for explaining them what the protocol was and for making them sign an informed consent. The procedure was agreed to be performed during the school time and inside the school facilities.

All the children were subjected to the same three-stage procedure: (1) Relaxing time with Meditation Music, (2) SART fixed version and (3) SART randomized version. See Figure 9.2.

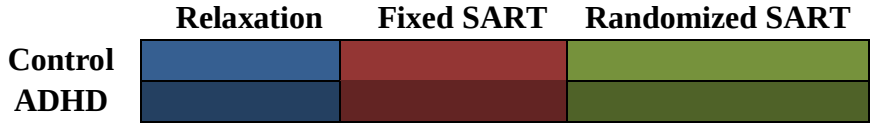

Figure 9.2. Classification of the data by type of participant and stage.

- **Relaxing time:** The child uses headphones and closes their eyes for about 5 minutes while relaxing music is reproduced. As all the sessions were taken inside the public school and there were noise everywhere, this was the most appropriated method detected for creating a base state during the procedure due to the hyperactive and/or inattentive nature of the children (See Figure 9.2).
- **SART fixed version:** The fixed version presents digits appearing in ascendant order from 1 to 9. The number of trials is 225, were the 10% corresponds to No-Go and the 90% corresponds to Go. The child can anticipate the response action required based on the fact that the emergence of the digits always happens in the same order. A break of not less than a minute was given to every child before the next task.
- **SART randomized version:** The randomized version presents digits appearing in disorder, following a pseudo-randomized distribution. The number of trials is 225, were the 10% corresponds to No-Go and the 90% corresponds to Go. See Figure 4. The child cannot anticipate the response action required based on the fact that the emergence of the digits is unpredictable, so the attention levels and velocity for responding have to be superior.

The Phase-Locking Value [43], a measure for likelihood, was utilized for analyzing correlations among the signals collected by the electrodes. The paradigm computed using the phase of the signal is introducing by Winfree [88] for studying the coupled-oscillators synchronization and the first representation of neural behavior through the action potential or Local Field Potentials (LFP).

The test responses introduced into the NEMA model for understanding the transitions between attentional and inattentional states. As EEG and behavioral data are collected and analyzed, these are also compared providing relevant information, regarding how neuroenergetics behave for both groups of children.

9.4 Data Collection

As there were plenty of limitations for working with the children, both instrumental and temporal, it is required to design an experiment capable of showing up important differences between both groups. The children's confidentiality and anonymity was guaranteed and the collected data only may be used for academic purposes. This study did not represent any harm to the participants, all of them participated voluntarily and they might leave at any time; at least one parent and the child provided verbal assent prior to the session beginning.

The study was conducted during the usual schooling time, implying standard conditions associated to the daily scholar tasks.

Each children was treated separately. The attentional data was collected using a psychological test in a computer for sensing sustained attention in a performing task; meanwhile, their EEG signals were collected using the Emotiv Epoc neuroheadset.

A standard positioning for the children was required for avoiding big differences in the electroencephalographic signal among stages. These differences might appear for electrode displacements on the scalp and also for a low transmission power of the Bluetooth connection.

9.5 Classification of the Data and Signal Processing

The data is clustered according to the group of study –control or ADHD- and the stage of the experiment –Relaxation, Fixed SART or Randomized SART- as it is shown in Figure 9.2.

Following this, each set is filtered with EEGLAB [89] FIR Butterworth filters in three different ranges of frequency: Theta (4-8 Hz) using a filter of order 78, SMR (12-15 Hz) and Beta (15-18 Hz). The latter two using a filter of order 98. See Figure 9.3 for the spectral maps in each case.

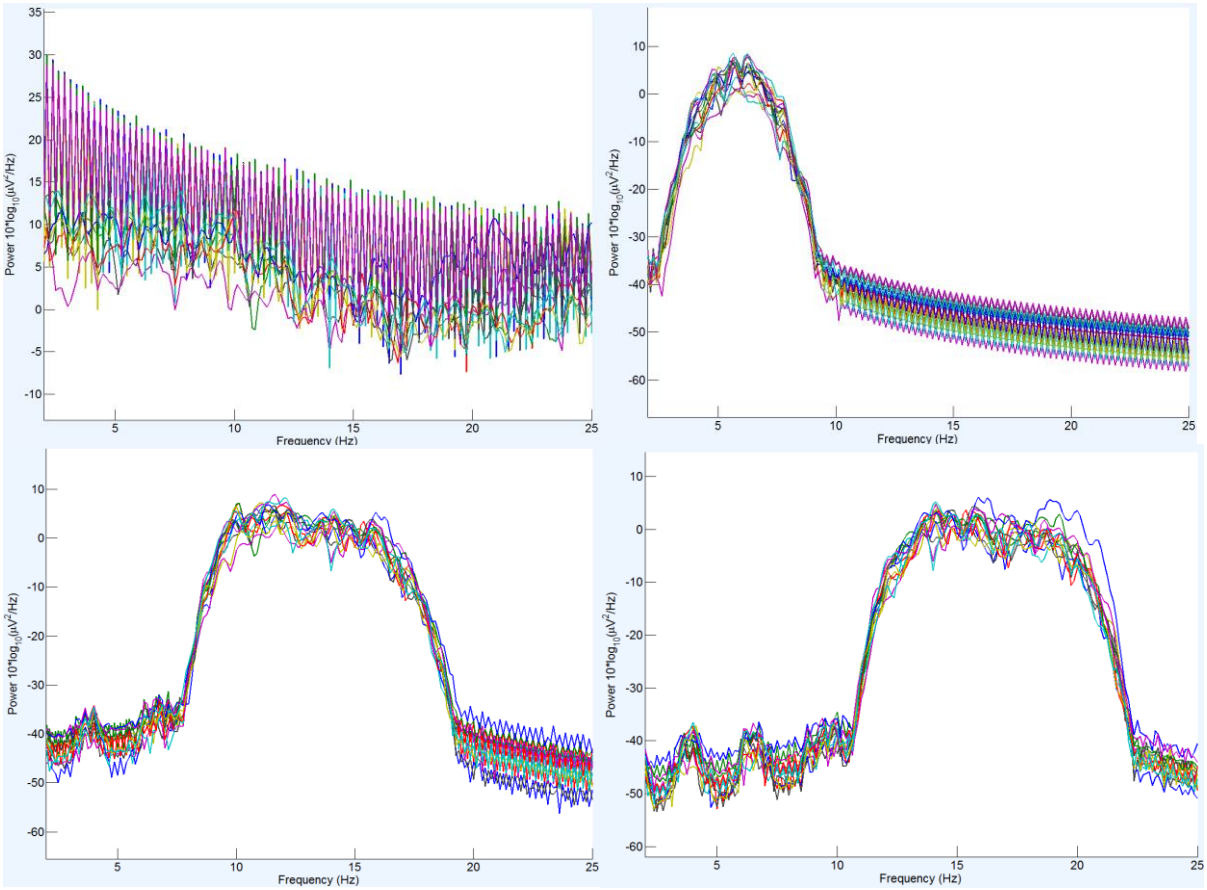

Figure 9.3. Spectral maps of EEG signals. Top left: Full signal. Top right: signal filtered in a 4-8 Hz frequency. Down left: signal filtered in a 12-15 Hz frequency. Down right: signal filtered in a 15-18 Hz frequency.

9.6 Graphs and Small-World Metrics

For plotting each graph and starting from its correspondent PLV matrix, the small-world metrics are obtained according to the following procedure:

- **Thresholding:** The threshold was set in a way that every node stayed connected in every network. All the values of the matrix below 0.15 (threshold) are transformed into 0.
- **Binarization:** The values different to 0 are transformed into 1.Small-world metrics calculation: The clustering coefficient, the global efficiency and the local efficiency are calculated for each node and then for the whole network, while the characteristic path length is calculated directly for the whole network. The small-world metrics were obtained using the Brain Connectivity Toolbox (BCT) [32].
- **Graph construction:** The electrodes are represented by nodes, and the synchronizations between two channels are depicted as edges. The edges ratios and its colors vary according to the local efficiency of the node as shown in Figure 9.4. $E(G_i)$ is the efficiency of the subgraph i, which is the node i.

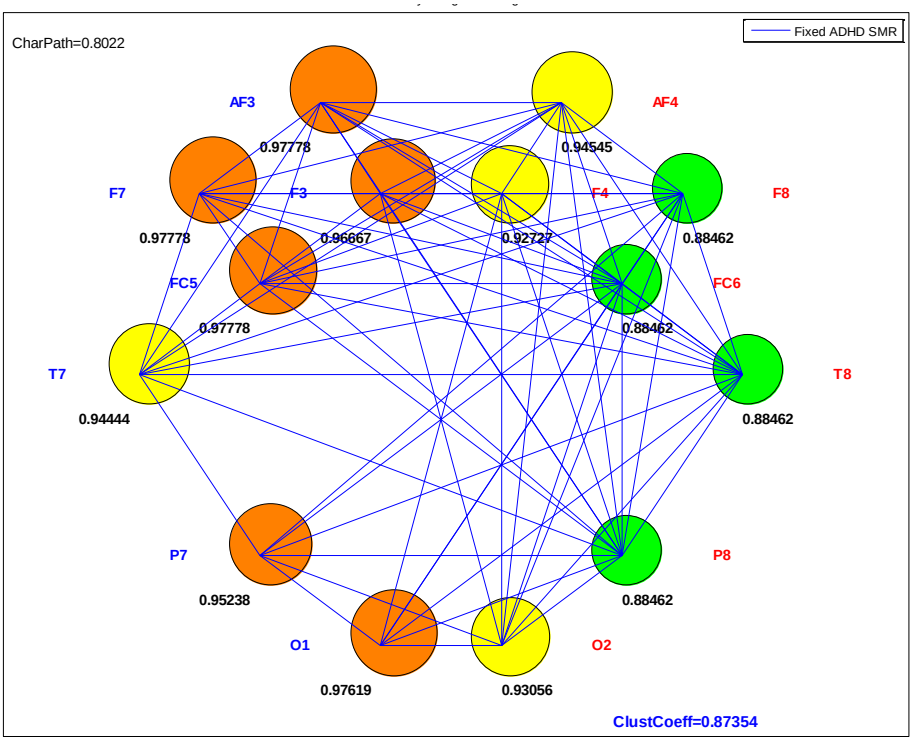

Figure 9.4. A graph with its small-network measurements constructed from the EEG signals collected.

10 Results

10.1 SART

As Figure 10.1 shows, both groups have good levels of attention for responding to stimuli successfully to more than a half of the trials, but have a lower performance in the random version. For control participants, the omission responses are 25,8% for fixed SART and 28,5% for randomized SART, increasing omissions a 2,70%. For ADHD participants, the percentages are 21,4% and 39,3% respectively, rising a 17,9%. This represents a gap between groups of 15,2%, pointing to a notable greater difficulty for ADHD children for transiting from the fixed test to the randomized test compared to control children.

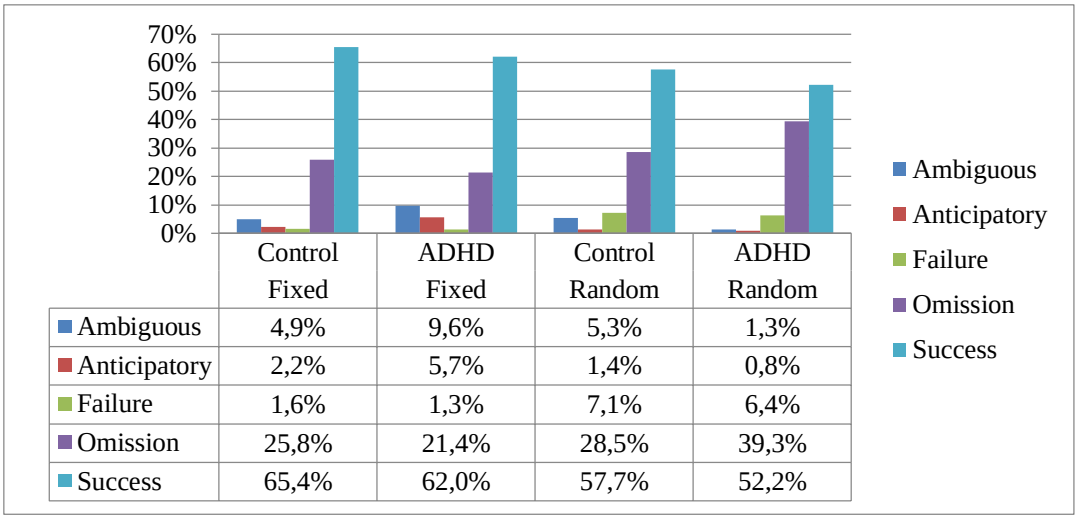

	Control Fixed	ADHD Fixed	Control Random	ADHD Random
Ambiguous	4,9%	9,6%	5,3%	1,3%
Anticipatory	2,2%	5,7%	1,4%	0,8%
Failure	1,6%	1,3%	7,1%	6,4%
Omission	25,8%	21,4%	28,5%	39,3%
Success	65,4%	62,0%	57,7%	52,2%

Figure 10.1. Classification of the SART responses for Control and ADHD participants.

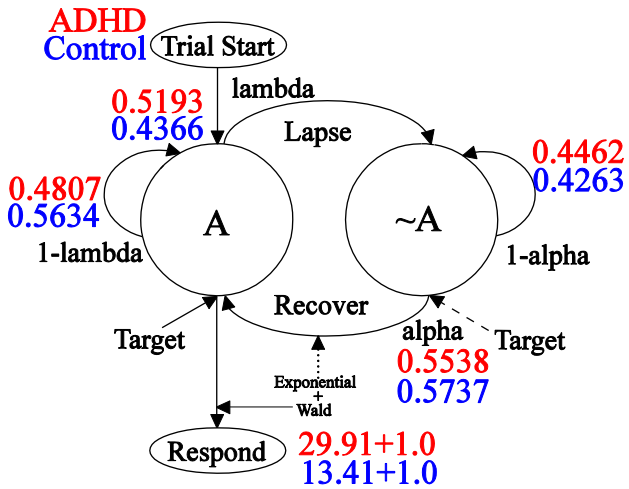

Figure 10.2. Markovian model from [78] included with the permission of the author. The outputs obtained for this experiment are written in blue for the control group and red for the ADHD group.

In
Figure *10.2*, the Markovian model is depicted. The code developed in LEM for each group can be found in Appendix B. The observed and estimated frequencies and the standard residual, are given according to the different combinations among the manifest variables: participant, stage, trial and response. The pseudo R-squared measures are calculated along with the log-linear parameters.

The conditional probabilities of P(Y|X) are the ones taken in consideration for representing the transitions between states in the model, due to X and Y are the latent variables. For each variable X (attention) and Y (inattention), two dimensions are correspondent: 1 is for transitioning to the other state and 2 is for transitioning to the same state. Thus, the transition 1|1 indicates that Y transitions to X, 2|1 indicates that Y transitions to itself, 1|2 indicates that X transitions to itself and 2|2 indicates that X transitions to Y.

The higher differences are evidenced for λ, where ADHD children have a probability of having a lapse of 51.93% and the 43.66% for control children. The probability of remaining in the attentional state is 48.07% and 56.34% for ADHD and control groups respectively. Between each pair of values a significant difference of 8.27% is noticed, which means that there is expected a higher chance of going from an attentional to an inattentional state for the ADHD group.

In α, the probability of recovering, there is a 55.38% for ADHD and 57.37% for control, having a difference of 1.99%. It represents a higher chance, but not very significant, for transitioning from an inattentive state to an attentive state in control children.

ADHD children have less probability to stay focus on SART trials, also they may stuck in mind wandering states with a lower probability for coming back to an attending state for an effective response. In the other hand, control children may leave the focus state but they are more likely to return to pay attention to the stimuli with less effort in comparison with ADHD children.

10.2 Small-Metrics for the Brainwaves

From the average PLV matrices obtained according to the group, stages and brainwaves, the small-world metrics are calculated. The clustering coefficient (C), characteristic path length (L) and global efficiency (E) are shown in Table 10.1 and Table 10.2.

	Control								
	Theta (4-8 Hz)			**SMR (12-15 Hz)**			**Beta (15-18 Hz)**		
	C	**L**	**E**	**C**	**L**	**E**	**C**	**L**	**E**
Relax	0,8818	0,7802	0,8901	0,8836	0,7912	0,8956	0,9159	0,8242	0,9121
Fixed	0,8766	0,8132	0,9066	0,8714	0,7912	0,8956	0,9627	0,956	0,978
Random	0,9052	0,8681	0,9341	0,8965	0,8571	0,9286	0,9627	0,956	0,978

Table 10.1. C, L and E calculated for Theta, SMR and Beta brainwaves

for every stage of the protocol in the control group.

	ADHD								
	Theta (4-8 Hz)			SMR (12-15 Hz)			Beta (15-18 Hz)		
	C	L	E	C	L	E	C	L	E
Relax	0,9324	0,8901	0,9451	0,8917	0,8352	0,9176	0,9426	0,8901	0,9451
Fixed	0,9799	0,978	0,989	0,9362	0,9231	0,9615	0,989	0,989	0,9945
Random	0,9127	0,8791	0,9396	0,8981	0,8462	0,9231	0,989	0,989	0,9945

Table 10.2. C, L and E calculated for Theta, SMR and Beta brainwaves for every stage of the protocol in the ADHD group.

10.2.1 Theta

Theta activity generally represents a more daydream like, fantasy prone rather spacey state of mind that is associated with mental inefficiency[90]. There are some significant differences for each group, as it is shown in Figure 10.3 and Table *10.3*:

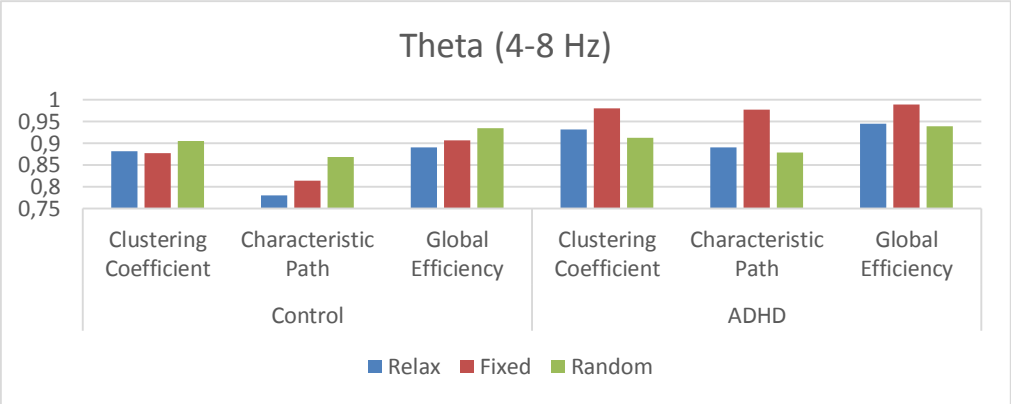

Figure 10.3. Comparison of network metrics for the Theta (4-8Hz) brainwave.

	Theta (4-8Hz)			
	Control		ADHD	
	C-L	Difference	C-L	Difference
Relax	10,16%	3,82%	4,23%	4,04%
Fixed	6,34%	2,63%	0,19%	-3,17%
Random	3,71%		3,36%	

Table 10.3. Percentual difference between C and L for each stage and the respective difference between the stages for the Theta (4-8Hz) brainwave.

- **Control:** The participants increase upwardly the quantity of resources placed at disposal, an expectable behavior for the ascendant requirement of abilities during the experiment. The difference between $C$and L for the relaxation stage is 10,16%, while in the fixed stage it is 6,34% and in the randomized stage it is a 3,71%, having a percentual difference of 3,82% between relaxed and fixed stages and 2,63% between fixed and randomized stages.

• **ADHD:** The quantity of resources placed at disposal increases as far as the fixed SART stage, but during the randomized SART, a decrement is evidenced in the three metrics despite the task difficulty. The difference between C and L for the relaxation stage is 4,23%, while in the fixed stage it is 0,19% and in the randomized stage it is a 3,36%, having a percentual difference of 4,04% between relaxed and fixed stages and -3,17% between fixed and randomized stages.

The connectivity in the ADHD group is always denser than the control group's. Even so, the connectivity in the control group increases stage by stage, while in the ADHD group increases from the relaxed stage to the fixed stage, but reduces from the fixed stage to the randomized stage. The full graphs may be seen in Appendix A.

10.2.2 SMR

The sensorimotor rhythm refers to the movement planning, which is the readiness of the neural network for performing an action. The higher the values, the less prepared the network is, as it is shown in Figure 10.4 and Table 10.4:

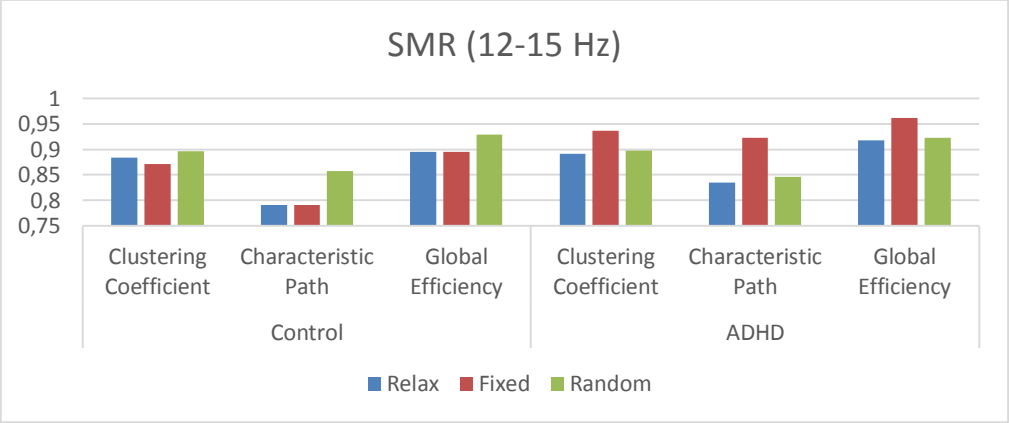

Figure 10.4. Comparison of network metrics for the SMR (12-15Hz) brainwave.

	SMR (12-15 Hz)			
	Control		ADHD	
	C-L	Difference	C-L	Difference
Relax	9,24%	1,22%	5,65%	4,34%
Fixed	8,02%	4,08%	1,31%	-3,88%
Random	3,94%		5,19%	

Table 10.4. Percentual difference between C and L for each stage and the respective difference between the stages for the SMR (12-15Hz) brainwave.

• **Control:** For the relaxation and the fixed SART stages, the connectivity levels are very much alike. This is due to the relaxation does not have any performance instruction and the fixed SART is a monotonous task, but in the randomized SART the connectivity ascends on

account of its complexity, giving place again to a predictable tendency. The difference between $C$and L for the relaxation stage is 9,24%, while in the fixed stage it is 8,02% and in the randomized stage it is a 3,94%, having a percentual difference of 1,22% between relaxed and fixed stages and 4,08% between fixed and randomized stages.

• **ADHD:** The SMR metrics in fixed SART are much higher than in the previous stage, and again it is considerably reduced in randomized SART, implying a great lack of movement planning. The difference between $C$and L for the relaxation stage is 5,65%, while in the fixed stage it is 1,31% and in the randomized stage it is a 5,19%, having a percentual difference of 4,34% between relaxed and fixed stages and -3,88% between fixed and randomized stages.

The connectivity in the ADHD group is always denser than the control group's. Even so, the connectivity in the control group remains almost the same from the relaxed stage to the fixed stage and increases from the fixed stage to the randomized stage, while in the ADHD group increases from the relaxed stage to the fixed stage, but reduces from the fixed stage to the randomized stage.

10.2.3 Beta

Reflects how desynchronized the active brain tissue is as the values are increased. It is also higher while the eyes of the participant are open, as it is shown in Figure 10.5 and Table 10.5:

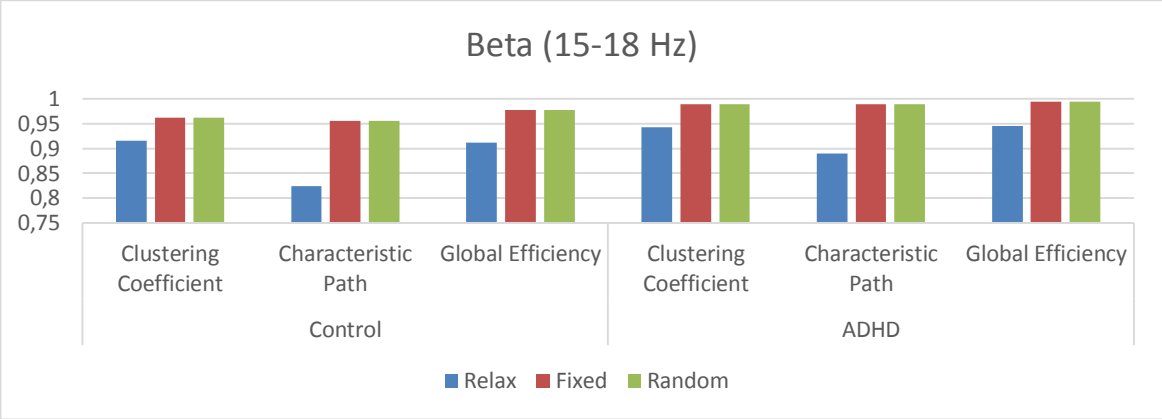

Figure 10.5. Comparison of network metrics for the Beta (15-18Hz) brainwave.

	Beta (15-18 Hz)			
	Control		ADHD	
	C-L	Difference	C-L	Difference
Relax	9,17%	8,50%	5,25%	5,25%
Fixed	0,67%	0,00%	0,00%	0,00%
Random	0,67%		0,00%	

Table 10.5. Percentual difference between C and L for each stage and the respective difference between the stages for the Beta (15-18Hz) brainwave.

- **Control:** For the relaxation stage, the closed-eyes stage, the connectivity is superior in the remaining stages. The difference between C and L for the relaxation stage is 9,17%, while in the fixed stage it is 0,67% and in the randomized stage it is a 0,67%, having a percentual difference of 8,50% between relaxed and fixed stages and 0,00% between fixed and randomized stages.

- **ADHD:** A similar tendency is evidenced in the ADHD groups, but the metrics have values a little lower. The difference between C and L for the relaxation stage is 5,25%, while in the fixed stage it is 0,00% and in the randomized stage it is a 0,00%, having a percentual difference of 5,25% between relaxed and fixed stages and 0,00% between fixed and randomized stages.

For the three brainwaves analyzed corresponding to the control group, the characteristic path length tends to be lower than the clustering coefficient and the global efficiency, denoting an organization in these graphs closer to the small-world networks type than the ADHD group, whose graph organization is closer to the organized networks type.

11 Discussion

The Neuroenergetics of Maintained Attention (NEMA) implied in tasks as SART may be explained using a Markov model, assuming the probability of lapses of attention from 1 s to the next, and the probability of drifting back to the attentional state. Their values are affected by the fatigue of the brain units (neurons and glia cells) as they traffic chemical-electric signals between. Also it determines the probability of the individual being inattentive at any point in time over the long run [78].

Markov models may be calculated on the assumption of latent or uncovered variables. Models of latent classes have been useful to identify and classify profiles of behavior according to internal syndromes, external syndromes and problems of the dream [91] and capabilities [92]. By the same procedure, it would be possible to characterize EEG brain functioning (latent) from manifest behavioral data [93, 94].

Despite ADHD does not have a unique profile nor a single explanation [95], as brain networks do not have an unique activation, few researchers report intra-subject variability [84]. Recently de Zeeuw, et al. [96] suggest at least three independent pathways involved in ADHD: a dorsal front striatal pathway involved in cognitive control, a ventral front striatal pathway involved in reward processing and a front cerebellar pathway related to temporal processing.

That finding should correspond to neural activations according with NET assumptions; also it would be expected different patterns of connectivity within ADHD and non-diagnosed children. Rhythms are activated in a deviated manner in ADHD, in easy tasks brain response with high activation and exaggerate energetic spending, passing the time the circuits do not have enough resources to maintain all frequencies activation, then brain deploy lower rhythms for keeping the rate activity in higher bands as it was demonstrated in [97].

We observed higher connectivity in Beta (15-18 Hz), then SMR (12-15 Hz) and lately in Theta (4-8 Hz). In theta, the declining of resources placed for disposal at the randomized SART stage might imply an issue regulating the production of required resources for the tasks fulfillment. In SMR, the metrics in fixed SART are higher than in relaxation, the previous stage. According to Killeen (2013) monotonous tasks are more demanding for these children due their susceptibility to keep moving between tasks. Surely, another pattern would be observed if the SART was a decreased difficulty test.

Synchronous activity of oscillating network is critical for coordinate behavior [98]; the level of interregional functional connectivity seems to be related to local band power as well as distance, long distance communication is mainly supported by synchronization in low frequency bands, like theta, while short distance local communication depends upon synchronization higher rhythms, as beta [99].

Neuroimaging techniques suggest that ADHD brains have lower connectivity between the bilateral VLPFC, the anterior cingulate cortex, the superior parietal lobule and the cerebellum during a working memory task compared to healthy controls [100]. Inattention and hyperactivity/impulsivity in ADHD are related to altered intrinsic connectivity in orbitofrontal-temporal-occipital and front-amygdala-occipital networks [101].

The enhanced connectivity at short-range within reward-motivation regions and their decreased connectivity with regions in long-range suggest impaired interactions between control and reward pathways in ADHD that might underlie attention and motivation deficits in ADHD [102]. ADHD might derive from deregulated modulation of cortical plasticity in the developing brain [103, 104].

12 Conclusions

The functional connectivity differences between ADHD children and control children were analyzed using an electroencephalographic low-cost neuroheadset. After the connectivity matrices and its respective network properties were computed through PLV, the data was transformed into functional connectivity graphs.

It was possible to evidence graphically and numerically the differences for each group and stage of the procedure in theta, SMR and beta brainwaves. For the limitations related to the number of channels and the resolution of the Emotiv Epoc, it was pivotal to make a comparative analysis with the results obtained from another source. In this case, the other source was the SART, which is a behavioral test for identifying omission responses, among others.

The NeT [78] stated a feeding neural circuit issue, but graphs and the small-world metrics suggest that it is originated due to energetic management: there is energy available but for some reason, the ADHD brain gamble all its resources in the first opportunity instead of save energy for later. It leads to build solid neural grids too early for learning the meaningful facts of the task, ADHD children invest more neural resources in the fixed SART stage and did not adjust brain rhythms in response to the randomized SART stage.

A study examining the power EEG [105], reported that ADHD subjects showed elevated coherence in the lower alpha (8 Hz) band and reduced coherence in the upper alpha (10–11 Hz) band; also the 8-Hz ADHD elevation and a 2- to 6-Hz control group coherence elevation were independent of stimulus presentation.

ADHD score was positively correlated with both the frequencies and mind-wandering responses [106]. It is suggested that the binding in mind wandering states and the misbalanced brain connectivity over time is on the administration (*i.e.* over-communication) of the transitions between bands according to environment challenges. The encoding approach leads to assume that an ADHD brain has difficulties to filter stimuli and controlling resources owing to a more deficient management of resources compared to a Control brain.

With clustering coefficient and characteristic path length metrics, it is possible identify to which kind of networks the graphs obtained are much alike. In this case, the control graphs for Theta and SMR brainwaves are closer to the small-world networks than other graphs obtained during the procedure. It might be because of the matrices obtained through the PLV had synchronizations in less nodes than in other cases, suggesting that probably these participants transited less times to the inattention state, as the Markov model explains.

13 Future Works

- "Sustained Attention in ADHD and Control Children using Event-Related Potential in a SART for Characterizing EEG Omission Responses in Both Groups": A synchronization between the behavioral test performance and the recording of the signal is required for getting the connectivity representations in each response.
  A mark has to be sent at the beginning and the end of each stages: relaxation, fixed SART and randomized SART. The synchronization has to be made using an extra application sub serving as a controller.
  Thus, it will make possible to ensure a characterization of the relevant responses in time represented through the graph theory measurements, and explained with the NeT.

- "Validation of the methodology using the Emotiv Epoc+ for the children in the Integral Audiology Institute in Pereira": A comparative study using an Emotiv Epoc neuroheadset with better resolution. This study is necessary for supporting the current results and give them a stronger background, by using a more representative sample and equipment more sophisticated.
  The children were diagnosed already and the contact with their parents is constant, making easier their monitoring.

- "A Low-cost Visualization Model for Sustained Attention in Real Time": A model for detecting in real time the capability of a subject for maintaining the sustained attention given a task. For being able to generating standard conditions, it is necessary to have a prior sample of both groups: ADHD and control for characterizing each group. The sample has to be big enough for being representative.
  According to the representative sample, it would be possible to generate an standard representation.

14 Bibliography

[1] H. Berger, "Über das Elektrenkephalogramm des Menschen," *Archiv für Psychiatrie und Nervenkrankheiten,* vol. 87, pp. 527-570, 1929/12/01 1929.

[2] D. C. Mowery, "Plus ca change: Industrial R&D in the “third industrial revolution”," *Industrial and Corporate Change,* January 12, 2009 2009.

[3] J. Greenwood, "The Third Industrial Revolution: Technology, Productivity, and Income Inequality," *Economic Review,* p. Q2, 1999.

[4] R. Kitchin, *The data revolution: Big data, open data, data infrastructures and their consequences*: Sage, 2014.

[5] A. Beaulieu, "Voxels in the brain: neuroscience, informatics and changing notions of objectivity," *Social studies of science,* vol. 31, pp. 635-680, 2001/10// 2001.

[6] M. Duvinage, T. Castermans, M. Petieau, T. Hoellinger, G. Cheron, and T. Dutoit. (2013, 2013). Performance of the Emotiv Epoc headset for P300-based applications. *Biomedical engineering online 12,* 56.

[7] A. L. S. Ferreira, L. C. d. Miranda, and E. E. C. d. Miranda, "Interfaces cérebro-computador de sistemas interativos: estado da arte e desafios de IHC," presented at the Proceedings of the 11th Brazilian Symposium on Human Factors in Computing Systems, Cuiaba, Brazil, 2012.

[8] K. Yaomanee, S. Pan-ngum, and P. I. N. Ayuthaya, "Brain signal detection methodology for attention training using minimal EEG channels," in *ICT and Knowledge Engineering (ICT & Knowledge Engineering), 2012 10th International Conference on*, 2012, pp. 84-89.

[9] I. OBJETIVO and I. M. LEGAL, "PLAN NACIONAL DE INTERVENCIÓN EN DISCAPACIDAD PLAN DE ACCIÓN 2005–2007."

[10] D. Pineda, F. Lopera, G. Henao, J. Palacio, and F. Castellanos, "Confirmación de la alta prevalencia del trastorno por déficit de atención en una comunidad colombiana," *Revista de neurología,* vol. 32, pp. 217-222, 2001.

[11] J. Cornejo, O. Osío, Y. Sánchez, J. Carrizosa, G. Sánchez, H. Grisales, *et al.*, "Prevalencia del trastorno por déficit de atención-hiperactividad en niños y adolescentes colombianos," *Rev Neurol,* vol. 40, pp. 716-722, 2005.

[12] A. P. Association, *Diagnostic and statistical manual of mental disorders, (DSM-5®)*: American Psychiatric Pub, 2013.

[13] R. A. Barkley, "Behavioral inhibition, sustained attention, and executive functions: constructing a unifying theory of ADHD," *Psychological bulletin,* vol. 121, p. 65, 1997.

[14] E. Bullmore and O. Sporns, "Complex brain networks: graph theoretical analysis of structural and functional systems," *Nat Rev Neurosci,* vol. 10, pp. 186-198, 03//print 2009.

[15] D. S. Bassett and E. Bullmore, "Small-world brain networks," *The neuroscientist,* vol. 12, pp. 512-523, 2006.

[16] Y. He, Z. Chen, G. Gong, and A. Evans, "Neuronal networks in Alzheimer's disease," *The Neuroscientist : a review journal bringing neurobiology, neurology and psychiatry,* vol. 15, pp. 333-350, 08/20/ 2009.

[17] Y. He and A. Evans, "Graph theoretical modeling of brain connectivity," *Current opinion in neurology,* vol. 23, pp. 341-350, 08/24/ 2010.

[18] O. Sporns, D. R. Chialvo, M. Kaiser, and C. C. Hilgetag, "Organization, development and function of complex brain networks," *Trends in Cognitive Sciences,* vol. 8, pp. 418-425, 9// 2004.

[19] C. Stam and J. Reijneveld, "Graph theoretical analysis of complex networks in the brain," *Nonlinear Biomedical Physics,* vol. 1, p. 3, // 2007.

[20] M. Bota and M. A. Arbib, "Integrating databases and expert systems for the analysis of brain structures: connections, similarities, and homologies," *Neuroinformatics,* vol. 2, pp. 19-58, 2004 2004.
[21] F. Crick and E. Jones, "Backwardness of human neuroanatomy," *Nature,* vol. 361, pp. 109-110, 1993/01// 1993.
[22] O. Sporns, G. Tononi, and R. Kötter, "The human connectome: A structural description of the human brain," *PLoS Comput. Biol.,* vol. 1, p. e42, 2005.
[23] V. J. Wedeen, R. P. Wang, J. D. Schmahmann, T. Benner, W. Y. I. Tseng, G. Dai, *et al.*, "Diffusion spectrum magnetic resonance imaging (DSI) tractography of crossing fibers," *NeuroImage,* vol. 41, pp. 1267-1277, 7/15/ 2008.
[24] P. Hagmann, M. Kurant, X. Gigandet, P. Thiran, V. J. Wedeen, R. Meuli, *et al.* (2007, 2007). Mapping human whole-brain structural networks with diffusion MRI. *PloS one 2(7),* e597.
[25] O. Sporns, *Discovering the Human Connectome*: The MIT Press, 2012.
[26] O. Sporns, *Networks of the Brain*: The MIT Press, 2010.
[27] M. F. Glasser and J. K. Rilling, "DTI Tractography of the Human Brain's Language Pathways," *Cerebral Cortex,* vol. 18, pp. 2471-2482, November 1, 2008 2008.
[28] B. Bernal and N. Altman, "The connectivity of the superior longitudinal fasciculus: a tractography DTI study," *Magnetic Resonance Imaging,* vol. 28, pp. 217-225, 2// 2010.
[29] H. Huang, J. Zhang, H. Jiang, S. Wakana, L. Poetscher, M. I. Miller, *et al.*, "DTI tractography based parcellation of white matter: Application to the mid-sagittal morphology of corpus callosum," *NeuroImage,* vol. 26, pp. 195-205, 5/15/ 2005.
[30] P. Olejniczak, "Neurophysiologic Basis of EEG," *Journal of Clinical Neurophysiology,* vol. 23, pp. 186-189, 2006.
[31] O. Sporns, "Brain connectivity," *Scholarpedia,* vol. 2, p. 4695, 2007.
[32] M. Rubinov and O. Sporns, "Complex network measures of brain connectivity: Uses and interpretations," *NeuroImage,* vol. 52, pp. 1059-1069, 9// 2010.
[33] W. de Haan, Y. Pijnenburg, R. Strijers, Y. van der Made, W. van der Flier, P. Scheltens, *et al.*, "Functional neural network analysis in frontotemporal dementia and Alzheimer's disease using EEG and graph theory," *BMC Neuroscience,* vol. 10, pp. 1-12, 2009/08/21 2009.
[34] C. J. Stam, W. de Haan, A. Daffertshofer, B. F. Jones, I. Manshanden, A. M. van Cappellen van Walsum, *et al.*, "Graph theoretical analysis of magnetoencephalographic functional connectivity in Alzheimer's disease," *Brain,* vol. 132, pp. 213-224, 2009-01-01 00:00:00 2009.
[35] E. J. Sanz-Arigita, M. M. Schoonheim, J. S. Damoiseaux, S. A. R. B. Rombouts, E. Maris, F. Barkhof, *et al.*, "Loss of 'Small-World' Networks in Alzheimer's Disease: Graph Analysis of fMRI Resting-State Functional Connectivity," *PLoS ONE,* vol. 5, p. e13788, 2010.
[36] S. C. Ponten, F. Bartolomei, and C. J. Stam, "Small-world networks and epilepsy: Graph theoretical analysis of intracerebrally recorded mesial temporal lobe seizures," *Clinical Neurophysiology,* vol. 118, pp. 918-927, 4// 2007.
[37] B. C. Bernhardt, Z. Chen, Y. He, A. C. Evans, and N. Bernasconi, "Graph-Theoretical Analysis Reveals Disrupted Small-World Organization of Cortical Thickness Correlation Networks in Temporal Lobe Epilepsy," *Cerebral Cortex,* vol. 21, pp. 2147-2157, September 1, 2011 2011.
[38] T. Wu, L. Wang, Y. Chen, C. Zhao, K. Li, and P. Chan, "Changes of functional connectivity of the motor network in the resting state in Parkinson's disease," *Neuroscience Letters,* vol. 460, pp. 6-10, 8/21/ 2009.
[39] K. T. E. Olde Dubbelink, A. Hillebrand, D. Stoffers, J. B. Deijen, J. W. R. Twisk, C. J. Stam, *et al.*, "Disrupted brain network topology in Parkinson's disease: a longitudinal magnetoencephalography study," *Brain,* 2013-11-22 00:00:00 2013.
[40] S. Debener, M. Ullsperger, M. Siegel, and A. K. Engel, "Single-trial EEG–fMRI reveals the dynamics of cognitive function," *Trends in Cognitive Sciences,* vol. 10, pp. 558-563, 12// 2006.

[41] C. J. Stam and B. W. van Dijk, "Synchronization likelihood: an unbiased measure of generalized synchronization in multivariate data sets," *Physica D: Nonlinear Phenomena,* vol. 163, pp. 236-251, 3/15/ 2002.
[42] C. J. Stam, G. Nolte, and A. Daffertshofer, "Phase lag index: Assessment of functional connectivity from multi channel EEG and MEG with diminished bias from common sources," *Human Brain Mapping,* vol. 28, pp. 1178-1193, 2007.
[43] J.-P. Lachaux, E. Rodriguez, J. Martinerie, and F. J. Varela, "Measuring phase synchrony in brain signals," *Human Brain Mapping,* vol. 8, pp. 194-208, 1999.
[44] R. Ramirez and Z. Vamvakousis, "Detecting Emotion from EEG Signals Using the Emotive Epoc Device," in *Brain Informatics*. vol. 7670, F. Zanzotto, S. Tsumoto, N. Taatgen, and Y. Yao, Eds., ed: Springer Berlin Heidelberg, 2012, pp. 175-184.
[45] H. Norhazman, N. M. Zaini, M. N. Taib, H. A. Omar, R. Jailani, S. Lias, *et al.*, "Behaviour of EEG Alpha Asymmetry when stress is induced and binaural beat is applied," in *Computer Applications and Industrial Electronics (ISCAIE), 2012 IEEE Symposium on*, 2012, pp. 297-301.
[46] N. Thakor, "Building Brain Machine Interfaces–Neuroprosthetic Control with Electrocorticographic Signals," *Newsletter,* vol. 2015, 2015.
[47] J.-P. Onnela, J. Saramäki, J. Kertész, and K. Kaski, "Intensity and coherence of motifs in weighted complex networks," *Physical Review E,* vol. 71, p. 065103, 06/13/ 2005.
[48] M. E. J. Newman, "Properties of highly clustered networks," *Physical Review E,* vol. 68, p. 026121, 08/21/ 2003.
[49] V. Latora and M. Marchiori, "Efficient Behavior of Small-World Networks," *Physical Review Letters,* vol. 87, p. 198701, 10/17/ 2001.
[50] A. J. Lawrence, A. W. Chung, R. G. Morris, H. S. Markus, and T. R. Barrick, "Structural network efficiency is associated with cognitive impairment in small-vessel disease," *Neurology,* vol. 83, pp. 304-311, 2014.
[51] S. Milgram, "The Small-World Problem," *Psychology Today,* vol. 1, 1967.
[52] M. Kochen, "Toward structural sociodynamics," *The Small,* pp. 52-64, 1989.
[53] B. Bollobás, "Random Graphs. 1985," *Academic, London,* 1985.
[54] L. Astolfi, F. De Vico Fallani, F. Cincotti, D. Mattia, M. G. Marciani, S. Bufalari, *et al.*, "Imaging functional brain connectivity patterns from high-resolution EEG and fMRI via graph theory," *Psychophysiology,* vol. 44, pp. 880-893, 2007.
[55] B. van Wijk, C. Stam, and A. Daffertshofer, "Comparing Brain Networks of Different Size and Connectivity Density Using Graph Theory," *PLoS ONE,* vol. 5, p. e13701, 10/28/ 2010.
[56] D. J. Watts and S. H. Strogatz, "Collective dynamics of 'small-world'networks," *nature,* vol. 393, pp. 440-442, 1998.
[57] L. A. N. Amaral and J. M. Ottino, "Complex networks," *The European Physical Journal B - Condensed Matter and Complex Systems,* vol. 38, pp. 147-162, 2004/03/01 2004.
[58] S. Boccaletti, V. Latora, Y. Moreno, M. Chavez, and D. U. Hwang, "Complex networks: Structure and dynamics," *Physics Reports,* vol. 424, pp. 175-308, 2// 2006.
[59] K. Heilman and E. Valenstein, "Clinical neuropsychology. Oxford University Press," *New York,* 1985.
[60] M. S. Gazzaniga, *The Cognitive Neurosciences*: MIT Press, 2000.
[61] F. Ferrerira-Santos, "Complex Network Analysis of Brain Connectivity: An Introduction," *University of Porto,* 2012.
[62] T. Montez, K. Linkenkaer-Hansen, B. W. van Dijk, and C. J. Stam, "Synchronization likelihood with explicit time-frequency priors," *NeuroImage,* vol. 33, pp. 1117-1125, 12// 2006.
[63] F. Bartolomei, I. Bosma, M. Klein, J. C. Baayen, J. C. Reijneveld, T. J. Postma, *et al.*, "Disturbed functional connectivity in brain tumour patients: Evaluation by graph analysis of synchronization matrices," *Clinical Neurophysiology,* vol. 117, pp. 2039-2049, 9// 2006.

[64] S. Micheloyannis, E. Pachou, C. J. Stam, M. Breakspear, P. Bitsios, M. Vourkas, *et al.*, "Small-world networks and disturbed functional connectivity in schizophrenia," *Schizophrenia Research*, vol. 87, pp. 60-66, 10// 2006.

[65] Q. Yu, J. Sui, S. Rachakonda, H. He, W. Gruner, G. Pearlson, *et al.*, "Altered Topological Properties of Functional Network Connectivity in Schizophrenia during Resting State: A Small-World Brain Network Study," *PLoS ONE*, vol. 6, p. e25423, 2011.

[66] G. Koutrika, F. A. Effendi, Zolt, #225, n. Gy, #246, *et al.*, "Combating spam in tagging systems," presented at the Proceedings of the 3rd international workshop on Adversarial information retrieval on the web, Banff, Alberta, Canada, 2007.

[67] F. Xing and W. Wang, "On the critical phase transition time of wireless multi-hop networks with random failures," presented at the Proceedings of the 14th ACM international conference on Mobile computing and networking, San Francisco, California, USA, 2008.

[68] C. J. Stam and J. C. Reijneveld. (2007, 2007). Graph theoretical analysis of complex networks in the brain. *Nonlinear biomedical physics 1(1)*, 3. Available: http://europepmc.org/abstract/MED/17908336

http://europepmc.org/articles/PMC1976403?pdf=render

http://europepmc.org/articles/PMC1976403

http://dx.doi.org/10.1186/1753-4631-1-3

[69] C. J. Stam, B. F. Jones, G. Nolte, M. Breakspear, and P. Scheltens, "Small-world networks and functional connectivity in Alzheimer's disease," *Cerebral cortex (New York, N.Y. : 1991)*, vol. 17, pp. 92-99, 2007/01// 2007.

[70] A. M. Lascano, S. Vulliemoz, G. Lantz, L. Spinelli, C. Michel, and M. Seeck, "A Review on Non-Invasive Localisation of Focal Epileptic Activity Using EEG Source Imaging."

[71] A. Pikovsky, M. Rosenblum, and J. Kurths, *Synchronization : a universal concept in nonlinear sciences*. Cambridge [etc.]: Cambridge University Press, 2001.

[72] W. J. Freeman, "Origin, structure, and role of background EEG activity. Part 3. Neural frame classification," *Clinical Neurophysiology*, vol. 116, pp. 1118-1129, 2005.

[73] A. Pikovsky and M. Rosenblum, "Synchronization," *Scholarpedia*, vol. 2, p. 1459, 2007.

[74] M. G. Rosenblum, A. Pikovsky, J. Kurths, C. Schäfer, and P. A. Tass, "Phase synchronization: from theory to data analysis," *Handbook of biological physics*, vol. 4, pp. 93-94, 2001.

[75] P. Ukeob, K. C. Veluvolu, and L. Minho, "Navigational/informational intent discrimination based on Phase Locking Value(PLV)," in *Brain-Computer Interface (BCI), 2014 International Winter Workshop on*, 2014, pp. 1-4.

[76] F. Mormann, K. Lehnertz, P. David, and C. E. Elger, "Mean phase coherence as a measure for phase synchronization and its application to the EEG of epilepsy patients," *Physica D: Nonlinear Phenomena*, vol. 144, pp. 358-369, 10/1/ 2000.

[77] R. D. Todd and K. N. Botteron, "Is attention-deficit/hyperactivity disorder an energy deficiency syndrome?," *Biological Psychiatry*, vol. 50, pp. 151-158, 8/1/ 2001.

[78] P. R. Killeen, "Absent without leave; a neuroenergetic theory of mind wandering," *Frontiers in Psychology*, vol. 4, p. 373, 2013.

[79] M. Bastian and J. Sackur, "Mind wandering at the fingertips: automatic parsing of subjective states based on response time variability," *Frontiers in Psychology*, vol. 4, p. 573, 09/05

06/07/received

08/11/accepted 2013.

[80] J. Geissler, M. Romanos, U. Hegerl, and T. Hensch, "Hyperactivity and sensation seeking as autoregulatory attempts to stabilize brain arousal in ADHD and mania?," *ADHD Attention Deficit and Hyperactivity Disorders*, vol. 6, pp. 159-173, 2014/09/01 2014.

[81] I. H. Robertson, T. Manly, J. Andrade, B. T. Baddeley, and J. Yiend, "`Oops!': Performance correlates of everyday attentional failures in traumatic brain injured and normal subjects," *Neuropsychologia,* vol. 35, pp. 747-758, 5/19/ 1997.
[82] K. A. Johnson, I. H. Robertson, S. P. Kelly, T. J. Silk, E. Barry, A. Dáibhis, *et al.*, "Dissociation in performance of children with ADHD and high-functioning autism on a task of sustained attention," *Neuropsychologia,* vol. 45, pp. 2234-2245, // 2007.
[83] S. Draine, "Inquisit. 3.0," ed: Seattle, WA: Millisecond Software, LLC, 2009.
[84] P. R. Killeen, V. A. Russell, and J. A. Sergeant, "A behavioral neuroenergetics theory of ADHD," *Neuroscience & Biobehavioral Reviews,* vol. 37, pp. 625-657, 2013.
[85] J. K. Vermunt, "LEM: Log-linear and event history analysis with missing data using the EM algorithm," Tilburg University, Work and Organization Research Centre1993.
[86] R. Lievesley, M. Wozencroft, and D. Ewins, "The Emotiv EPOC neuroheadset: an inexpensive method of controlling assistive technologies using facial expressions and thoughts?," *Journal of Assistive Technologies,* vol. 5, pp. 67-82, 2011.
[87] N. A. Badcock, P. Mousikou, Y. Mahajan, P. de Lissa, J. Thie, and G. McArthur, "Validation of the Emotiv EPOC® EEG gaming system for measuring research quality auditory ERPs," *PeerJ,* vol. 1, p. e38, 2013.
[88] A. T. Winfree, *The geometry of biological time*. Berlin [etc.]: Springer, 1980.
[89] A. Delorme and S. Makeig, "EEGLAB: an open source toolbox for analysis of single-trial EEG dynamics including independent component analysis," *Journal of Neuroscience Methods,* vol. 134, pp. 9-21, 3/15/ 2004.
[90] S. Warner, "Cheat Sheet for Neurofeedback," ed, 2013.
[91] C. R. C. López, A. M. Rivas, and L. O. Zarate, "Modelos de clases latentes para definir perfiles conductuales en niños de 4 y 5 años," *Revista Electrónica de Psicología Iztacala,* vol. 14, p. 17, 2011.
[92] J. K. Vermunt, "Multilevel latent variable modeling: An application in education testing," *Austrian Journal of Statistics,* vol. 37, pp. 285-299, 2008.
[93] R. Ratcliff and F. Tuerlinckx, "Estimating parameters of the diffusion model: Approaches to dealing with contaminant reaction times and parameter variability," *Psychonomic Bulletin & Review,* vol. 9, pp. 438-481, 2002.
[94] D. Matzke and E.-J. Wagenmakers, "Psychological interpretation of the ex-Gaussian and shifted Wald parameters: A diffusion model analysis," *Psychonomic Bulletin & Review,* vol. 16, pp. 798-817, 2009.
[95] P. Killeen, R. Tannock, and T. Sagvolden, "The Four Causes of ADHD: A Framework," in *Behavioral Neuroscience of Attention Deficit Hyperactivity Disorder and Its Treatment*. vol. 9, C. Stanford and R. Tannock, Eds., ed: Springer Berlin Heidelberg, 2012, pp. 391-425.
[96] P. de Zeeuw, J. Weusten, S. van Dijk, J. van Belle, and S. Durston, "Deficits in Cognitive Control, Timing and Reward Sensitivity Appear to be Dissociable in ADHD," *PLoS ONE,* vol. 7, p. e51416, 2012.
[97] A. Baroni and F. X. Castellanos, "Neuroanatomic and cognitive abnormalities in attention-deficit/hyperactivity disorder in the era of 'high definition' neuroimaging," *Current Opinion in Neurobiology,* vol. 30, pp. 1-8, 2// 2015.
[98] G. Buzsáki and A. Draguhn, "Neuronal Oscillations in Cortical Networks," *Science,* vol. 304, pp. 1926-1929, 2004.
[99] C. J. Stam and E. C. W. van Straaten, "The organization of physiological brain networks," *Clinical Neurophysiology,* vol. 123, pp. 1067-1087, 6// 2012.
[100] K. Konrad and S. B. Eickhoff, "Is the ADHD brain wired differently? A review on structural and functional connectivity in attention deficit hyperactivity disorder," *Human Brain Mapping,* vol. 31, pp. 904-916, 2010.

[101] L. Cocchi, I. E. Bramati, A. Zalesky, E. Furukawa, L. F. Fontenelle, J. Moll, *et al.*, "Altered Functional Brain Connectivity in a Non-Clinical Sample of Young Adults with Attention-Deficit/Hyperactivity Disorder," *The Journal of Neuroscience*, vol. 32, pp. 17753-17761, 2012.
[102] D. Tomasi and N. D. Volkow, "Abnormal Functional Connectivity in Children with Attention-Deficit/Hyperactivity Disorder," *Biological Psychiatry*, vol. 71, pp. 443-450, 3/1/ 2012.
[103] C. Liston, M. M. Cohen, T. Teslovich, D. Levenson, and B. J. Casey, "Atypical Prefrontal Connectivity in Attention-Deficit/Hyperactivity Disorder: Pathway to Disease or Pathological End Point?," *Biological Psychiatry*, vol. 69, pp. 1168-1177, 6/15/ 2011.
[104] D. A. Fair, J. Posner, B. J. Nagel, D. Bathula, T. G. C. Dias, K. L. Mills, *et al.*, "Atypical Default Network Connectivity in Youth with Attention-Deficit/Hyperactivity Disorder," *Biological Psychiatry*, vol. 68, pp. 1084-1091, 12/15/ 2010.
[105] M. Murias, J. M. Swanson, and R. Srinivasan, "Functional Connectivity of Frontal Cortex in Healthy and ADHD Children Reflected in EEG Coherence," *Cerebral Cortex*, vol. 17, pp. 1788-1799, 2007.
[106] M. S. Franklin, M. D. Mrazek, C. L. Anderson, C. Johnston, J. Smallwood, A. Kingstone, *et al.*, "Tracking Distraction: The Relationship Between Mind-Wandering, Meta-Awareness, and ADHD Symptomatology," *Journal of Attention Disorders*, 2014.

A. Appendix

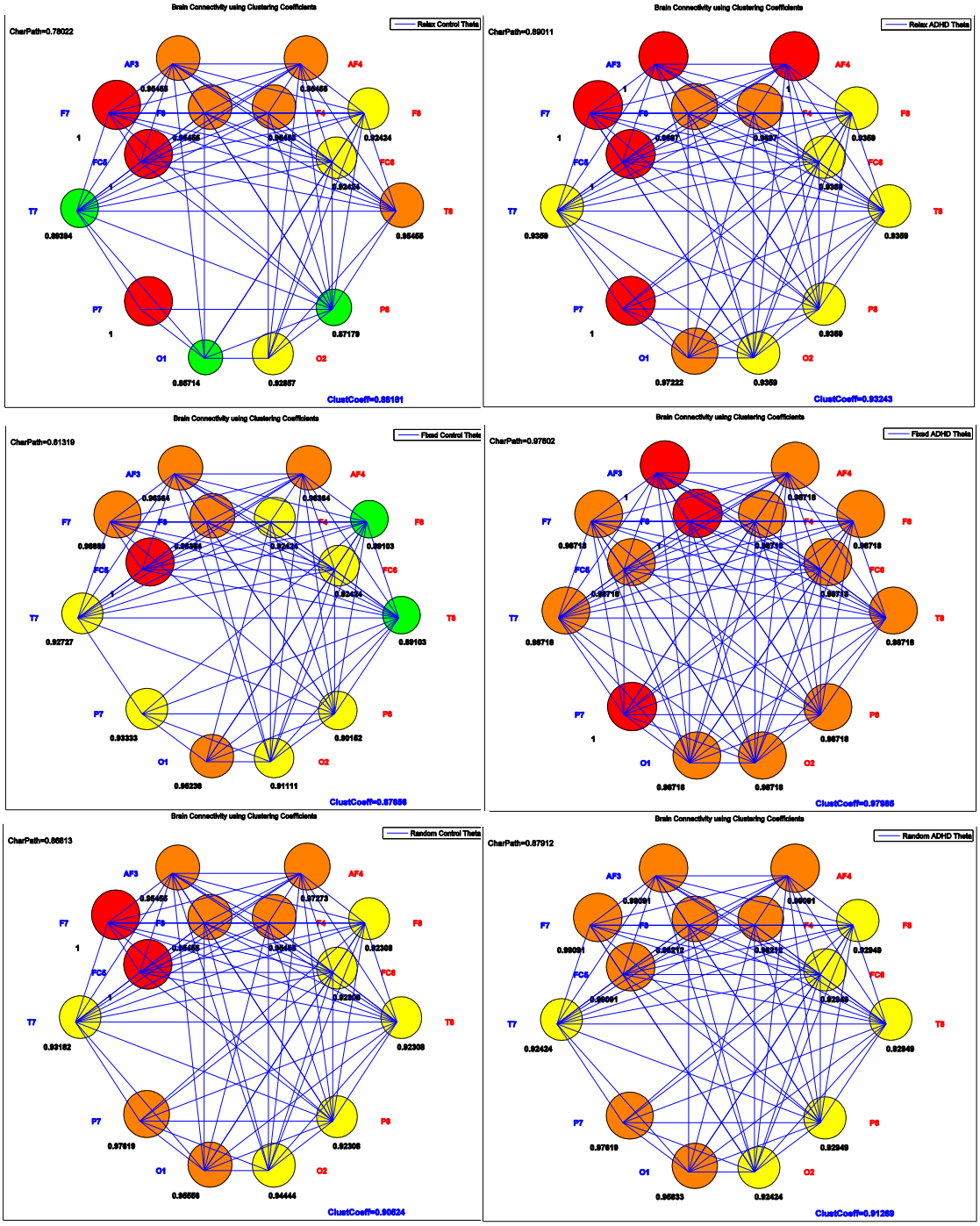

Figure A.1. Average graphs for the Theta (4-8Hz) brainwave. (1) Top left: Relaxation stage for control group. (2) Top Right: Relaxation stage for ADHD group. (3) Center left: Fixed SART stage for control group. (4) Center right: Fixed SART for ADHD group. (5) Down left: Randomized SART for control group. (6) Down right: Randomized SART for ADHD group.

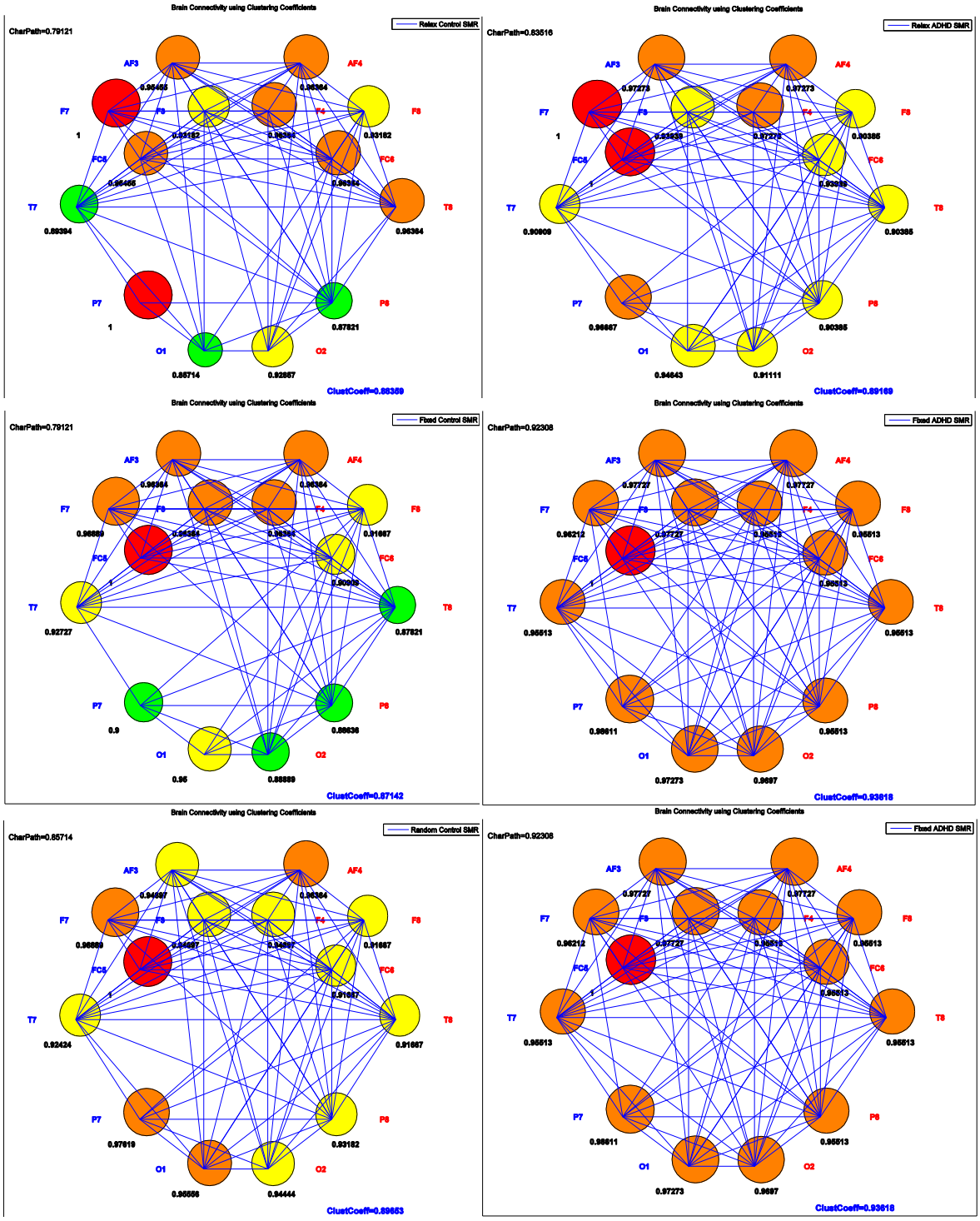

Figure A.2. Average graphs for the SMR (12-15Hz) brainwave. (1) Top left: Relaxation stage for control group. (2) Top Right: Relaxation stage for ADHD group. (3) Center left: Fixed SART stage for control group. (4) Center right: Fixed SART for ADHD group. (5) Down left: Randomized SART for control group. (6) Down right: Randomized SART for ADHD group.

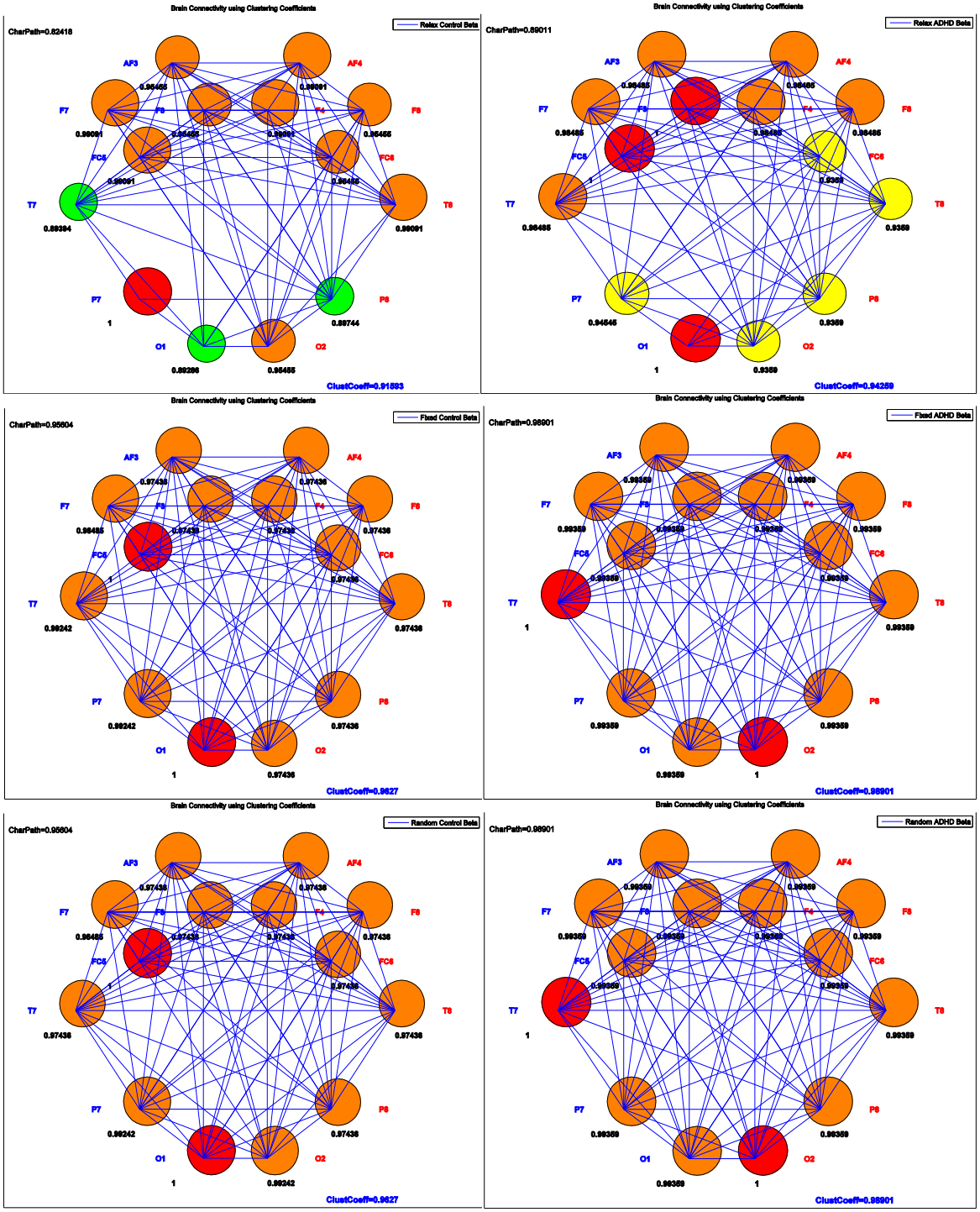

Figure A.3. Average graphs for the Beta (15-18Hz) brainwave. (1) Top left: Relaxation stage for control group. (2) Top Right: Relaxation stage for ADHD group. (3) Center left: Fixed SART stage for control group. (4) Center right: Fixed SART for ADHD group. (5) Down left: Randomized SART for control group. (6) Down right: Randomized SART for ADHD group.

B. Appendix

B.1. LEM output for the ADHD group using the Markovian model

*** STATISTICS ***

Number of iterations = 56
Converge criterion = 0.0000006802
Seed random values = 1030

X-squared = 471.9072 (0.0000)
L-squared = 462.7508 (0.0000)
Cressie-Read = 456.9670 (0.0000)
Dissimilarity index = 0.1709
Degrees of freedom = 173
Log-likelihood = -9538.18808
Number of parameters = 23 (+4)
Sample size = 2260.0
BIC(L-squared) = -873.3490
AIC(L-squared) = 116.7508
BIC(log-likelihood) = 19254.0079
AIC(log-likelihood) = 19122.3762

Eigenvalues information matrix
1809.6032 158.1929 82.8692 32.2581 5.0532 1.3585
0.4973 0.2371 0.1214 0.0000 -0.0000 -0.0001
-0.0003 -0.0007

WARNING: 5 (nearly) boundary or non-identified (log-linear) parameters

*** FREQUENCIES ***

P S T R	observed	estimated	std. res.
1 1 1 1	3.050	3.545	-0.263
1 1 1 2	1.050	1.748	-0.528
1 1 1 3	0.050	0.045	0.023
1 1 1 4	59.050	36.665	3.697
1 1 1 5	36.050	57.306	-2.808
1 1 2 1	0.050	0.050	0.001
1 1 2 2	0.050	0.049	0.003
1 1 2 3	0.050	4.418	-2.078
1 1 2 4	0.050	0.050	0.001
1 1 2 5	13.050	8.625	1.507
1 2 1 1	7.050	3.523	1.879
1 2 1 2	0.050	1.738	-1.280
1 2 1 3	0.050	0.278	-0.433
1 2 1 4	24.050	36.410	-2.048
1 2 1 5	68.050	57.359	1.412
1 2 2 1	0.050	0.050	0.001
1 2 2 2	0.050	0.049	0.003
1 2 2 3	3.050	4.418	-0.651
1 2 2 4	0.050	0.050	0.001
1 2 2 5	10.050	8.625	0.485
2 1 1 1	4.050	3.545	0.268
2 1 1 2	3.050	1.748	0.985
2 1 1 3	0.050	0.045	0.023
2 1 1 4	30.050	36.665	-1.092
2 1 1 5	62.050	57.306	0.627
2 1 2 1	0.050	0.050	0.001
2 1 2 2	0.050	0.049	0.003
2 1 2 3	3.050	4.418	-0.651
2 1 2 4	0.050	0.050	0.001
2 1 2 5	10.050	8.625	0.485
2 2 1 1	5.050	3.523	0.813
2 2 1 2	1.050	1.738	-0.522
2 2 1 3	0.050	0.278	-0.433
2 2 1 4	28.050	36.410	-1.386
2 2 1 5	65.050	57.359	1.016
2 2 2 1	0.050	0.050	0.001
2 2 2 2	0.050	0.049	0.003
2 2 2 3	3.050	4.418	-0.651
2 2 2 4	0.050	0.050	0.001
2 2 2 5	10.050	8.625	0.485
3 1 1 1	6.050	3.545	1.330
3 1 1 2	3.050	1.748	0.985
3 1 1 3	0.050	0.045	0.023
3 1 1 4	16.050	36.665	-3.405
3 1 1 5	74.050	57.306	2.212
3 1 2 1	0.050	0.050	0.001
3 1 2 2	0.050	0.049	0.003
3 1 2 3	1.050	4.418	-1.602
3 1 2 4	0.050	0.050	0.001
3 1 2 5	12.050	8.625	1.166
3 2 1 1	16.050	3.523	6.674
3 2 1 2	8.050	1.738	4.788
3 2 1 3	0.050	0.278	-0.433
3 2 1 4	15.050	36.410	-3.540
3 2 1 5	60.050	57.359	0.355
3 2 2 1	0.050	0.050	0.001
3 2 2 2	0.050	0.049	0.003
3 2 2 3	3.050	4.418	-0.651
3 2 2 4	0.050	0.050	0.001
3 2 2 5	10.050	8.625	0.485
4 1 1 1	0.050	3.545	-1.856
4 1 1 2	3.050	1.748	0.985
4 1 1 3	0.050	0.045	0.023
4 1 1 4	55.050	36.665	3.036
4 1 1 5	41.050	57.306	-2.147
4 1 2 1	0.050	0.050	0.001
4 1 2 2	0.050	0.049	0.003
4 1 2 3	3.050	4.418	-0.651
4 1 2 4	0.050	0.050	0.001
4 1 2 5	10.050	8.625	0.485
4 2 1 1	1.050	3.523	-1.318
4 2 1 2	0.050	1.738	-1.280
4 2 1 3	0.050	0.278	-0.433
4 2 1 4	22.050	36.410	-2.380
4 2 1 5	76.050	57.359	2.468
4 2 2 1	0.050	0.050	0.001
4 2 2 2	0.050	0.049	0.003
4 2 2 3	1.050	4.418	-1.602
4 2 2 4	0.050	0.050	0.001
4 2 2 5	12.050	8.625	1.166
5 1 1 1	13.050	3.545	5.048
5 1 1 2	6.050	1.748	3.255
5 1 1 3	0.050	0.045	0.023
5 1 1 4	12.050	36.665	-4.065
5 1 1 5	68.050	57.306	1.419
5 1 2 1	0.050	0.050	0.001
5 1 2 2	0.050	0.049	0.003
5 1 2 3	0.050	4.418	-2.078

5 1 2 4	0.050	0.050	0.001
5 1 2 5	13.050	8.625	1.507
5 2 1 1	0.050	3.523	-1.850
5 2 1 2	0.050	1.738	-1.280
5 2 1 3	0.050	0.278	-0.433
5 2 1 4	28.050	36.410	-1.386
5 2 1 5	71.050	57.359	1.808
5 2 2 1	0.050	0.050	0.001
5 2 2 2	0.050	0.049	0.003
5 2 2 3	1.050	4.418	-1.602
5 2 2 4	0.050	0.050	0.001
5 2 2 5	12.050	8.625	1.166
6 1 1 1	1.050	3.577	-1.336
6 1 1 2	1.050	1.763	-0.537
6 1 1 3	0.050	0.046	0.021
6 1 1 4	66.050	36.991	4.778
6 1 1 5	32.050	57.815	-3.389
6 1 2 1	0.050	0.050	-0.001
6 1 2 2	0.050	0.050	0.001
6 1 2 3	3.050	4.457	-0.667
6 1 2 4	0.050	0.050	-0.001
6 1 2 5	10.050	8.701	0.457
6 2 1 1	0.050	3.555	-1.859
6 2 1 2	0.050	1.753	-1.286
6 2 1 3	2.050	0.281	3.340
6 2 1 4	59.050	36.734	3.682
6 2 1 5	39.050	57.869	-2.474
6 2 2 1	0.050	0.050	-0.001
6 2 2 2	0.050	0.050	0.001
6 2 2 3	10.050	4.457	2.649
6 2 2 4	0.050	0.050	-0.001
6 2 2 5	3.050	8.701	-1.916
7 1 1 1	2.050	3.577	-0.807
7 1 1 2	1.050	1.763	-0.537
7 1 1 3	0.050	0.046	0.021
7 1 1 4	40.050	36.991	0.503
7 1 1 5	57.050	57.815	-0.101
7 1 2 1	0.050	0.050	-0.001
7 1 2 2	0.050	0.050	0.001
7 1 2 3	9.050	4.457	2.175
7 1 2 4	0.050	0.050	-0.001
7 1 2 5	4.050	8.701	-1.577
7 2 1 1	1.050	3.555	-1.328
7 2 1 2	1.050	1.753	-0.531
7 2 1 3	0.050	0.281	-0.435
7 2 1 4	51.050	36.734	2.362
7 2 1 5	47.050	57.869	-1.422
7 2 2 1	0.050	0.050	-0.001
7 2 2 2	0.050	0.050	0.001
7 2 2 3	3.050	4.457	-0.667
7 2 2 4	0.050	0.050	-0.001
7 2 2 5	10.050	8.701	0.457
8 1 1 1	1.050	3.577	-1.336
8 1 1 2	0.050	1.763	-1.290
8 1 1 3	0.050	0.046	0.021
8 1 1 4	43.050	36.991	0.996
8 1 1 5	56.050	57.815	-0.232
8 1 2 1	0.050	0.050	-0.001
8 1 2 2	0.050	0.050	0.001
8 1 2 3	7.050	4.457	1.228
8 1 2 4	0.050	0.050	-0.001
8 1 2 5	6.050	8.701	-0.899
8 2 1 1	3.050	3.555	-0.268
8 2 1 2	1.050	1.753	-0.531
8 2 1 3	0.050	0.281	-0.435
8 2 1 4	25.050	36.734	-1.928
8 2 1 5	71.050	57.869	1.733
8 2 2 1	0.050	0.050	-0.001
8 2 2 2	0.050	0.050	0.001
8 2 2 3	9.050	4.457	2.175
8 2 2 4	0.050	0.050	-0.001
8 2 2 5	4.050	8.701	-1.577
9 1 1 1	6.050	3.577	1.308
9 1 1 2	5.050	1.763	2.475
9 1 1 3	0.050	0.046	0.021
9 1 1 4	53.050	36.991	2.640
9 1 1 5	36.050	57.815	-2.862
9 1 2 1	0.050	0.050	-0.001
9 1 2 2	0.050	0.050	0.001
9 1 2 3	9.050	4.457	2.175
9 1 2 4	0.050	0.050	-0.001
9 1 2 5	4.050	8.701	-1.577
9 2 1 1	0.050	3.555	-1.859
9 2 1 2	0.050	1.753	-1.286
9 2 1 3	0.050	0.281	-0.435
9 2 1 4	53.050	36.734	2.692
9 2 1 5	47.050	57.869	-1.422
9 2 2 1	0.050	0.050	-0.001
9 2 2 2	0.050	0.050	0.001
9 2 2 3	5.050	4.457	0.281
9 2 2 4	0.050	0.050	-0.001
9 2 2 5	8.050	8.701	-0.221
10 1 1 1	1.050	3.577	-1.336
10 1 1 2	0.050	1.763	-1.290
10 1 1 3	0.050	0.046	0.021
10 1 1 4	18.050	36.991	-3.114
10 1 1 5	81.050	57.815	3.056
10 1 2 1	0.050	0.050	-0.001
10 1 2 2	0.050	0.050	0.001
10 1 2 3	9.050	4.457	2.175
10 1 2 4	0.050	0.050	-0.001
10 1 2 5	4.050	8.701	-1.577
10 2 1 1	0.050	3.555	-1.859
10 2 1 2	0.050	1.753	-1.286
10 2 1 3	0.050	0.281	-0.435
10 2 1 4	36.050	36.734	-0.113
10 2 1 5	64.050	57.869	0.813
10 2 2 1	0.050	0.050	-0.001
10 2 2 2	0.050	0.050	0.001
10 2 2 3	6.050	4.457	0.754
10 2 2 4	0.050	0.050	-0.001
10 2 2 5	7.050	8.701	-0.560

*** PSEUDO R-SQUARED MEASURES ***

* P(X|ST) *

	baseline	fitted	R-squared
entropy	0.3700	0.0259	0.9300
qualitative variance	0.1068	0.0043	0.9601
classification error	0.1215	0.0043	0.9647
-2/N*log-likelihood	0.7400	0.0518	0.9300/0.4077
likelihood^(-2/N)	2.0959	1.0531	0.4975/0.9515

* P(Y|X) *

	baseline	fitted	R-squared
entropy	0.6929	0.6918	0.0016
qualitative variance	0.2499	0.2493	0.0023
classification error	0.4896	0.4765	0.0267

-2/N*log-likelihood	1.3859	1.3836 0.0016/0.0023
likelihood^(-2/N)	3.9983	3.9891 0.0023/0.0030

* P(R|X) *

	baseline	fitted	R-squared
entropy	0.9844	0.8550	0.1315
qualitative variance	0.2738	0.2603	0.0494
classification error	0.4137	0.4137	-0.0000
-2/N*log-likelihood	1.9688	1.7099	0.1315/0.2056
likelihood^(-2/N)	7.1622	5.5287	0.2281/0.2651

* P(P) *

	baseline	fitted	R-squared
entropy	2.3026	2.3026	-0.0000
qualitative variance	0.4500	0.4500	0.0000
classification error	0.8996	0.8996	0.0000
-2/N*log-likelihood	4.6052	4.6052	0.0000/0.0000
likelihood^(-2/N)	99.9980	99.9980	0.0000/0.0000

*** LOG-LINEAR PARAMETERS ***

* TABLE XST [or P(X|ST)] *

effect	beta	std err	z-value	exp(beta)	Wald	df	prob
X							
1	-0.0000			1.0000			
2	6.6018	1.4174	4.658	736.3962	21.69	1	0.000
XS							
1 1	0.0000			1.0000			
1 2	0.0000			1.0000			
2 1	0.0000			1.0000			
2 2	-1.8262	1.5510	-1.177	0.1610	1.39	1	0.239
XT							
1 1	0.0000			1.0000			
1 2	-0.0000			1.0000			
2 1	0.0000			1.0000			
2 2	-18.5959	******	*****	8.39E-0009	0.00	1	1.000
XST							
1 1 1	0.0000			1.0000			
1 1 2	0.0000			1.0000			
1 2 1	0.0000			1.0000			
1 2 2	-0.0000			1.0000			
2 1 1	0.0000			1.0000			
2 1 2	-0.0000			1.0000			
2 2 1	0.0000			1.0000			
2 2 2	1.7227	******	*****	5.5994	0.00	1	1.000

* TABLE XY [or P(Y|X)] *

effect	beta	std err	z-value	exp(beta)	Wald	df	prob
Y							
1	0.0000			1.0000			
2	-0.2160	******	*****	0.8057	0.00	1	1.000
XY							
1 1	0.0000			1.0000			
1 2	0.0000			1.0000			
2 1	0.0000			1.0000			
2 2	0.2933	******	*****	1.3408	0.00	1	1.000

* TABLE XR [or P(R|X)] *

effect	beta	std err	z-value	exp(beta)	Wald	df	prob
R							
1	0.0000			1.0000			
2	-0.0075	1.4107	-0.005	0.9925			
3	4.4873	1.0020	4.478	88.8824			
4	-0.0009	1.4099	-0.001	0.9991			
5	5.1562	0.9993	5.160	173.5102	98.23	4	0.000
XR							
1 1	0.0000			1.0000			
1 2	0.0000			1.0000			
1 3	0.0000			1.0000			
1 4	0.0000			1.0000			
1 5	0.0000			1.0000			
2 1	-0.0000			1.0000			
2 2	-0.7001	1.4266	-0.491	0.4965			
2 3	-72.8744	******	*****	2.24E-0032			
2 4	2.3371	1.4157	1.651	10.3516			
2 5	-2.3749	1.0073	-2.358	0.0930	29.91	4	0.000

*** (CONDITIONAL) PROBABILITIES ***

* P(X|ST) *

1 | 1 1	0.0014	(0.0019)
1 | 1 2	1.0000	(0.0000)
1 | 2 1	0.0084	(0.0053)
1 | 2 2	1.0000	(0.0000)
2 | 1 1	0.9986	(0.0019)
2 | 1 2	0.0000	(0.0000)
2 | 2 1	0.9916	(0.0053)
2 | 2 2	0.0000	(0.0000)

* P(Y|X) *

1 | 1	0.5538	(0.0000)
2 | 1	0.4462	(0.0000)
1 | 2	0.4807	(0.0000)
2 | 2	0.5193	(0.0000)

* P(R|X) *

1 | 1	0.0038	(0.0037)
2 | 1	0.0037	(0.0037)
3 | 1	0.3349	(0.0291)
4 | 1	0.0038	(0.0038)
5 | 1	0.6538	(0.0293)
1 | 2	0.0357	(0.0042)
2 | 2	0.0176	(0.0030)
3 | 2	0.0000	(0.0000) *
4 | 2	0.3697	(0.0109)
5 | 2	0.5769	(0.0111)

* P(P) *

1	0.0996
2	0.0996
3	0.0996
4	0.0996
5	0.0996
6	0.1004
7	0.1004
8	0.1004
9	0.1004
10	0.1004

*** LATENT CLASS OUTPUT ***

	X 1 Y 1	X 1 Y 2	X 2 Y 1	X 2 Y 2
	0.0673	0.0542	0.4223	0.4562
P 1	0.0996	0.0996	0.0996	0.0996
P 2	0.0996	0.0996	0.0996	0.0996
P 3	0.0996	0.0996	0.0996	0.0996
P 4	0.0996	0.0996	0.0996	0.0996
P 5	0.0996	0.0996	0.0996	0.0996
P 6	0.1004	0.1004	0.1004	0.1004
P 7	0.1004	0.1004	0.1004	0.1004
P 8	0.1004	0.1004	0.1004	0.1004
P 9	0.1004	0.1004	0.1004	0.1004
P 10	0.1004	0.1004	0.1004	0.1004
S 1	0.4873	0.4873	0.5018	0.5018
S 2	0.5127	0.5127	0.4982	0.4982
T 1	0.0353	0.0353	1.0000	1.0000
T 2	0.9647	0.9647	0.0000	0.0000
R 1	0.0038	0.0038	0.0357	0.0357
R 2	0.0037	0.0037	0.0176	0.0176
R 3	0.3349	0.3349	0.0000	0.0000
R 4	0.0038	0.0038	0.3697	0.3697
R 5	0.6538	0.6538	0.5769	0.5769

*** STATISTICS ***

Number of iterations = 151
Converge criterion = 0.0000009321
Seed random values = 4377

X-squared = 546.1794 (0.0000)
L-squared = 547.5519 (0.0000)
Cressie-Read = 533.7574 (0.0000)
Dissimilarity index = 0.2853
Degrees of freedom = 78
Log-likelihood = -4113.79533
Number of parameters = 18 (+4)
Sample size = 1130.0
BIC(L-squared) = -0.7860
AIC(L-squared) = 391.5519
BIC(log-likelihood) = 8354.1302
AIC(log-likelihood) = 8263.5907

Eigenvalues information matrix
788.1846 149.6064 53.5485 33.0836 0.7239 0.5295
0.1970 0.1075 0.0497 0.0337 0.0000 0.0000
-0.0000 -0.0000

WARNING: 5 (nearly) boundary or non-identified (log-linear) parameters

*** FREQUENCIES ***

P S T R	observed	estimated	std. res.
1 1 1 1	12.050	8.400	1.259
1 1 1 2	8.050	4.026	2.005
1 1 1 3	0.050	0.068	-0.070
1 1 1 4	8.050	27.981	-3.768
1 1 1 5	71.050	58.732	1.607
1 1 2 1	0.050	0.055	-0.020
1 1 2 2	0.050	0.052	-0.009
1 1 2 3	1.050	4.705	-1.685
1 1 2 4	0.050	0.070	-0.076
1 1 2 5	12.050	8.310	1.297
1 2 1 1	22.050	8.424	4.695
1 2 1 2	14.050	4.038	4.983
1 2 1 3	0.050	0.039	0.055
1 2 1 4	14.050	28.060	-2.645
1 2 1 5	49.050	58.847	-1.277
1 2 2 1	0.050	0.046	0.020
1 2 2 2	0.050	0.048	0.010
1 2 2 3	2.050	4.745	-1.237
1 2 2 4	0.050	0.039	0.058
1 2 2 5	11.050	8.314	0.949
2 1 1 1	16.050	8.400	2.639
2 1 1 2	5.050	4.026	0.510
2 1 1 3	0.050	0.068	-0.070
2 1 1 4	2.050	27.981	-4.902
2 1 1 5	76.050	58.732	2.260
2 1 2 1	0.050	0.055	-0.020
2 1 2 2	0.050	0.052	-0.009
2 1 2 3	3.050	4.705	-0.763
2 1 2 4	0.050	0.070	-0.076
2 1 2 5	10.050	8.310	0.604
2 2 1 1	2.050	8.424	-2.196
2 2 1 2	1.050	4.038	-1.487
2 2 1 3	0.050	0.039	0.055
2 2 1 4	80.050	28.060	9.815
2 2 1 5	16.050	58.847	-5.579
2 2 2 1	0.050	0.046	0.020
2 2 2 2	0.050	0.048	0.010
2 2 2 3	1.050	4.745	-1.696
2 2 2 4	0.050	0.039	0.058
2 2 2 5	12.050	8.314	1.296
3 1 1 1	2.050	8.438	-2.199
3 1 1 2	4.050	4.044	0.003
3 1 1 3	0.050	0.069	-0.071
3 1 1 4	16.050	28.106	-2.274
3 1 1 5	77.050	58.993	2.351
3 1 2 1	0.050	0.055	-0.021
3 1 2 2	0.050	0.052	-0.010
3 1 2 3	0.050	4.726	-2.151
3 1 2 4	0.050	0.070	-0.077
3 1 2 5	13.050	8.347	1.628
3 2 1 1	4.050	8.461	-1.517
3 2 1 2	0.050	4.055	-1.989
3 2 1 3	0.050	0.039	0.054
3 2 1 4	13.050	28.185	-2.851
3 2 1 5	83.050	59.109	3.114
3 2 2 1	0.050	0.046	0.019
3 2 2 2	0.050	0.048	0.009
3 2 2 3	9.050	4.766	1.962
3 2 2 4	0.050	0.039	0.057
3 2 2 5	4.050	8.351	-1.488

E = 0.4781, lambda = 0.1209

B.2. LEM output for the control group using the Markovian model

4 1 1 1	4.050	8.475	-1.520
4 1 1 2	1.050	4.062	-1.495
4 1 1 3	0.050	0.069	-0.072
4 1 1 4	9.050	28.230	-3.610
4 1 1 5	86.050	59.255	3.481
4 1 2 1	0.050	0.055	-0.022
4 1 2 2	0.050	0.052	-0.011
4 1 2 3	8.050	4.747	1.516
4 1 2 4	0.050	0.071	-0.078
4 1 2 5	5.050	8.384	-1.151
4 2 1 1	19.050	8.499	3.619
4 2 1 2	5.050	4.073	0.484
4 2 1 3	0.050	0.040	0.053
4 2 1 4	6.050	28.310	-4.184
4 2 1 5	70.050	59.370	1.386
4 2 2 1	0.050	0.046	0.018
4 2 2 2	0.050	0.048	0.008
4 2 2 3	12.050	4.787	3.319
4 2 2 4	0.050	0.039	0.056
4 2 2 5	1.050	8.388	-2.534
5 1 1 1	3.050	8.475	-1.864
5 1 1 2	2.050	4.062	-0.998
5 1 1 3	0.050	0.069	-0.072
5 1 1 4	64.050	28.230	6.742
5 1 1 5	31.050	59.255	-3.664
5 1 2 1	0.050	0.055	-0.022
5 1 2 2	0.050	0.052	-0.011
5 1 2 3	5.050	4.747	0.139
5 1 2 4	0.050	0.071	-0.078
5 1 2 5	8.050	8.384	-0.115
5 2 1 1	0.050	8.499	-2.898
5 2 1 2	0.050	4.073	-1.993
5 2 1 3	0.050	0.040	0.053
5 2 1 4	69.050	28.310	7.657
5 2 1 5	31.050	59.370	-3.675
5 2 2 1	0.050	0.046	0.018
5 2 2 2	0.050	0.048	0.008
5 2 2 3	6.050	4.787	0.577
5 2 2 4	0.050	0.039	0.056
5 2 2 5	7.050	8.388	-0.462

*** PSEUDO R-SQUARED MEASURES ***

* P(X|ST) *

	baseline	fitted	R-squared
entropy	0.3631	0.0128	0.9648
qualitative variance	0.1041	0.0018	0.9825
classification error	0.1181	0.0018	0.9845
-2/N*log-likelihood	0.7262	0.0256	0.9648/0.4120
likelihood^(-2/N)	2.0672	1.0259	0.5037/0.9757

* P(Y|X) *

	baseline	fitted	R-squared
entropy	0.6848	0.6847	0.0000
qualitative variance	0.2458	0.2458	0.0000
classification error	0.4353	0.4353	0.0000
-2/N*log-likelihood	1.3695	1.3695	0.0000/0.0000
likelihood^(-2/N)	3.9335	3.9333	0.0000/0.0001

* P(R|X) *

	baseline	fitted	R-squared
entropy	1.1037	0.9726	0.1188
qualitative variance	0.2866	0.2753	0.0394
classification error	0.4035	0.4035	-0.0000
-2/N*log-likelihood	2.2075	1.9452	0.1188/0.2078
likelihood^(-2/N)	9.0929	6.9952	0.2307/0.2592

* P(P) *

	baseline	fitted	R-squared
entropy	1.6094	1.6094	-0.0000
qualitative variance	0.4000	0.4000	0.0000
classification error	0.7991	0.7991	-0.0000
-2/N*log-likelihood	3.2189	3.2189	-0.0000/-0.0000
likelihood^(-2/N)	24.9996	24.9996	-0.0000/-0.0000

*** LOG-LINEAR PARAMETERS ***

* TABLE XST [or P(X|ST)] *

effect	beta	std err	z-value	exp(beta)	Wald	df	prob
X							
1	0.0000			1.0000			
2	6.2564	1.8649	3.355	521.3239	11.26	1	0.001
XS							
1 1	0.0000			1.0000			
1 2	0.0000			1.0000			
2 1	0.0000			1.0000			
2 2	0.5593	2.7269	0.205	1.7494	0.04	1	0.837
XT							
1 1	0.0000			1.0000			
1 2	0.0000			1.0000			
2 1	0.0000			1.0000			
2 2	-11.0134	******	*****	1.65E-0005	0.00	1	1.000
XST							
1 1 1	0.0000			1.0000			
1 1 2	0.0000			1.0000			
1 2 1	0.0000			1.0000			
1 2 2	0.0000			1.0000			
2 1 1	0.0000			1.0000			
2 1 2	0.0000			1.0000			
2 2 1	0.0000			1.0000			
2 2 2	-17.1966	******	*****	3.40E-0008	0.00	1	1.000

* TABLE XY [or P(Y|X)] *

effect	beta	std err	z-value	exp(beta)	Wald	df	prob
Y							
1	0.0000			1.0000			
2	-0.2971	******	*****	0.7429	0.00	1	1.000
XY							
1 1	0.0000			1.0000			
1 2	0.0000			1.0000			
2 1	0.0000			1.0000			
2 2	0.0420	******	*****	1.0429	0.00	1	1.000

* TABLE XR [or P(R|X)] *

effect	beta	std err	z-value	exp(beta)	Wald	df	prob
R							
1	0.0000			1.0000			
2	0.0464	2.1367	0.022	1.0475			
3	4.6443	1.5588	2.979	103.9923			
4	-0.1663	2.3454	-0.071	0.8468			
5	5.2051	1.5536	3.350	182.2043	39.25	4	0.000
XR							
1 1	0.0000			1.0000			

1 2	0.0000		1.0000			
1 3	-0.0000		1.0000			
1 4	0.0000		1.0000			
1 5	0.0000		1.0000			
2 1	-0.0000		1.0000			
2 2	-0.7819	2.1464	-0.364	0.4575		
2 3	-85.9915	******	*****	4.51E-0038		
2 4	1.3696	2.3495	0.583	3.9340		
2 5	-3.2624	1.5585	-2.093	0.0383	13.41	4 0.009

*** (CONDITIONAL) PROBABILITIES ***

* P(X|ST) *

1 | 1 1	0.0019	(0.0036)
1 | 1 2	0.9915	(0.0157)
1 | 2 1	0.0011	(0.0022)
1 | 2 2	1.0000	(0.0000)
2 | 1 1	0.9981	(0.0036)
2 | 1 2	0.0085	(0.0157)
2 | 2 1	0.9989	(0.0022)
2 | 2 2	0.0000	(0.0000)

* P(Y|X) *

1 | 1	0.5737	(0.0000)
2 | 1	0.4263	(0.0000)
1 | 2	0.5634	(0.0000)
2 | 2	0.4366	(0.0000)

* P(R|X) *

1 | 1	0.0035	(0.0054)
2 | 1	0.0036	(0.0054)
3 | 1	0.3597	(0.0422)
4 | 1	0.0029	(0.0052)
5 | 1	0.6303	(0.0422)
1 | 2	0.0848	(0.0088)
2 | 2	0.0407	(0.0063)
3 | 2	0.0000	(0.0000) *
4 | 2	0.2826	(0.0143)
5 | 2	0.5919	(0.0156)

* P(P) *

1	0.1991
2	0.1991
3	0.2000
4	0.2009
5	0.2009

*** LATENT CLASS OUTPUT ***

	X 1 Y 1	X 1 Y 2	X 2 Y 1	X 2 Y 2
	0.0678	0.0503	0.4969	0.3850
P 1	0.1991	0.1991	0.1991	0.1991
P 2	0.1991	0.1991	0.1991	0.1991
P 3	0.2000	0.2000	0.2000	0.2000
P 4	0.2009	0.2009	0.2009	0.2009
P 5	0.2009	0.2009	0.2009	0.2009
S 1	0.4994	0.4994	0.4996	0.4996
S 2	0.5006	0.5006	0.5004	0.5004
T 1	0.0112	0.0112	0.9994	0.9994
T 2	0.9888	0.9888	0.0006	0.0006
R 1	0.0035	0.0035	0.0848	0.0848
R 2	0.0036	0.0036	0.0407	0.0407
R 3	0.3597	0.3597	0.0000	0.0000
R 4	0.0029	0.0029	0.2826	0.2826
R 5	0.6303	0.6303	0.5919	0.5919

E = 0.4361, lambda = 0.1331

C. Appendix

Fragment of the code for the visualization tool developed using the BCT toolbox [32].

```
sizeImage=2500;
standardSize=500;
numElectrodes=14;


for j=1:1%7
   for i=1:1%3
   Graph(i,j).W=PhaseLockingValue1(i,j).NBT_theta.PLV;


for x=1:14
    for y=1:14
       if x==y
          Graph(i,j).W(x,y)=0;
       else if x>y
          Graph(i,j).W(x,y)=Graph(i,j).W(y,x);
          end
       end
    end
 end

 Graph(i,j).threshold=0.15
 Graph(i,j).CIJ_RAND=Graph(i,j).W;
 Graph(i,j).WIJ=threshold_absolute(Graph(i,j).CIJ_RAND,Graph(i).threshold);
 Graph(i,j).BIJ=weight_conversion(Graph(i,j).WIJ,'binarize');
   [Graph(i,j).lambda,Graph(i,j).efficiency,Graph(i,j).ecc,Graph(i,j).radius,Graph(i,j).diameter] =
charpath(Graph(i,j).BIJ);

  Graph(i,j).ClusteringCoef = clustering_coef_bu(Graph(i,j).BIJ);
  Graph(i,j).LocalEfficiency=efficiency_bin(Graph(i,j).BIJ,1);
  Graph(i,j).GlobalEfficiency=efficiency_bin(Graph(i,j).BIJ,0);

 Graph(i,j).ClusteringGlobal=sum(Graph(i,j).ClusteringCoef(1:14))/14;

figure

Coord1(1:14,1)=[3;1;4;2;0;2;4;6;8;10;8;6;9;7]*100+175;%+50;%+100.5;
Coord1(1:14,2)=(sizeImage/2.5)-[0;1;1;2;3;5;6;6;5;3;2;1;1;0]*150;%-50;%+150.5;
Electrodes=[1;2;3;4;5;6;7;8;9;10;11;12;13;14];
Electrodes=['AF3';'F7 ';'F3 ';'FC5';'T7 ';'P7 ';'O1 ';'O2 ';'P8 ';'T8 ';'FC6';'F4 ';'F8 ';'AF4'];
Electrodes=cellstr(Electrodes);

rectangle('Position',[0,0,1500,1200],'Curvature',[0,0],...
        'FaceColor','w')
daspect([1,1,1])

for k=1:numElectrodes
```

```
 if (Graph(1,i).LocalEfficiency(k)==1)
        colores='r';
    elseif (Graph(1,i).LocalEfficiency(k)>0.95)
        colores=[1 .5 0];
    elseif  (Graph(1,i).LocalEfficiency(k)>0.9)
        colores='y';
    elseif (Graph(1,i).LocalEfficiency(k)>0.85)
        colores='g';
    elseif (Graph(1,i).LocalEfficiency(k)>0.8)
        colores='b';
    else
        colores='black';
 end

 rectangle('Position',[Coord1(k,1),Coord1(k,2),standardSize*0.3,standardSize*0.3],'Curvature',[1,1],...
         'FaceColor',colores)%'g')

daspect([1,1,1])
if (k<8)
   text(Coord1(k,1)-50,Coord1(k,2)-25,strcat('
',num2str(Graph(i,j).ClusteringCoef(k))),'FontWeight','bold','FontSize',11)
   text(Coord1(k,1)-100,Coord1(k,2)+50,Electrodes(k),'Color','b','FontWeight','bold','FontSize',11)
else
   text(Coord1(k,1)+50,Coord1(k,2)-25,strcat('
',num2str(Graph(i,j).ClusteringCoef(k))),'FontWeight','bold','FontSize',11)
   text(Coord1(k,1)+200,Coord1(k,2)+50,Electrodes(k),'Color','r','FontWeight','bold','FontSize',11)
end
end
axis off
hold on

title('Brain Connectivity using Clustering Coefficients');
hold on;

[X,Y]=adjacency_plot_und(Graph(i,j).BIJ,Coord1+50);

plot(X,Y);
 hold off
 labelgraph=legend([stages{i} ' ' subjects{j}]);%[type(subject)]);
 text(15,1150,strcat('CharPath=',num2str(Graph(i,j).lambda)),'FontSize',11);


text(1010,25,strcat('ClustCoeff=',num2str(sum(Graph(i,j).ClusteringCoef(1:14))/14)),'Color','b','FontWeight','bold','F
ontSize',12);
   end
end
```